UNIVERSITY OF CALIFORNIA
Los Angeles

Laser cooling Yb^+ ions with optical frequency comb

A dissertation submitted in partial satisfaction
of the requirements for the degree
Doctor of Philosophy in Physics

by

Michael Ip

2018

ABSTRACT OF THE DISSERTATION

Laser cooling Yb^+ ions with optical frequency comb

by

Michael Ip

Doctor of Philosophy in Physics

University of California, Los Angeles, 2018

Professor Wesley C. Campbell, Chair

Trapped atomic ions are a multifaceted platform that can serve as a quantum information processor, precision measurement tool and sensor. However, in order to perform these experiments, the trapped ions need to be cooled substantially below room temperature. Doppler cooling has been a tremendous work horse in the ion trapping community. Hydrogen-like ions are good candidates because they have typically have a simple closed cycling transition that requires only a few lasers to Doppler cool. The ^{2}S to ^{2}P transition for these ions however typically lies in the UV to deep UV regime which makes buying a standard CW laser difficult as optical power here is hard to come by. Rather using a CW laser, which requires frequency stabilization and produces low optical power, this thesis explores how a mode-locked laser in the comb regime Doppler cools Yb ions. This thesis explores how a mode-locked laser is able to laser cool trapped ions and the consequences of using a broad spectrum light source. I will first give an overview of the architecture of our oblate Paul trap. Then I will discuss how a 10 picosecond optical pulse with a repetition rate of 80 MHz interacts with a 20 MHz linewidth $^2S_{1/2}$ to $^2P_{1/2}$ transition. Next I will go over our experiment involving ultrafast Ramsey experiment between the $^2S_{1/2}$ and $^2P_{1/2}$ states. Finally, I will present the results of these experi-

ments.

The dissertation of Michael Ip is approved.

Eric R. Hudson

Robert N. Candler

Wesley C. Campbell, Committee Chair

University of California, Los Angeles

2018

To my mom and dad .

TABLE OF CONTENTS

LIST OF FIGURES

LIST OF TABLES

ACKNOWLEDGMENTS

Graduate school is a long and difficult road. Before starting graduate school, I had the impression that grad school is just an extension to undergrad; thinking that the path to obtaining a Phd would be a clear cut path. It turns out that this is entirely incorrect. Grad school for me, and I'm sure for many others as well, is a journey where one has to struggle immensely intellectually and emotionally. I've learned that in order to get past these struggles, I had to rely on other people's help either in the lab or outside the lab.

I'd like to first thank my advisor Wes Campbell for being an extremely supportive advisor. Before joining the Campbell lab, I had one leg out the door of grad school. Late into my second year was when I first met Wes, even though he first thought I was an undergrad, was when I told myself I would give physics grad school one last shot. He told me I'd be his first grad student, and it's going to be a learning experience for the both of us. Luckily, thanks to Wes' patience, perseverance, and guidance, I am able to make it to the finish line and finish graduate school. He never gave up on his students, even when we were struggling. Obviously he is intellectually qualified to be a PI, but more importantly, he has the compassion for his students to be qualified to be a great PI.

It was joining the Campbell lab that refueled my passion for physics. Partly because of the interesting physics research that was being done, but more importantly, it was the people that inspired me to want to do the research. It's the wacky ideas our lab would have at lunch and dinner that would continue to drive the motivation to do research. The one with the wackiest ideas would be none other than my lab partner Anthony Ransford. Without Ransford's help along the way, we wouldn't have awesome software

control where we could sit in front of a computer and control our ions with a click of a button. But more importantly, it wouldn't have been as fun to do all this work without him.

I'd also like to thank everyone in the Campbell lab, Xueping Long, Gary Chen, Conrad Roman, Andrew Jayich, Tiangang Yang and David Hucul. I've received help throughout these years from each and every single one of them. As Wes has always said, AMO is a team effort, and none of our experiments could be done individually. That would also be a very boring experiment to work on if one were to work alone without a lab partner. I was very lucky to have landed in a group where we all jived with each other. The lab culture that existed in the Campbell group was an important factor to make the long and dry journey of graduate school bearable during the roughest times. Without all the fun jokes and pranks we would put play on Xueping, it probably would've added a few more years to my graduate school journey. I am very grateful to have worked with these guys and wouldn't switch any of them out for anyone else.

Outside of the lab, I would like to first thank my family for supporting me throughout these years. Especially my parents and my brother, for providing emotional support when the times were dark. It's their unconditional love that also helped carried me to the finish line for graduate school.

Last but not least, I would like to thank all my friends who have been there for me. Hector Garcia Vasquez, Patrick Vasquez, Kim Phifer, Alden Fan, Emily Martin, Amanda Freise, Alex Cahill, Keith Landry, Louis Yang and Shan Jiang. I'd like to also thank Jill Murrin for the patience and support she showed for me.

CHAPTER 1

Ion trapping

Radio frequency Paul traps have revolutionized atomic physics by confining a single charged particle, or more, in a small region of space for an indefinite period of time.[17] With the right combination of alternating electric fields and DC electric fields, this creates a stability region which can confine particles with the appropriate charge to mass ratio. Alternatively, the particles that do not have the appropriate charge to mass ratio will be filtered out of the trap. A mass spectrometer is a 2D rf Paul trap that does not have endcaps along the axial direction.

The levitation of the charged particles in free space provides an environment which is superior to other platforms, as there is no physical heat bath that the ion is connected to. This is ideal because this gives rise to a system that has low entropy. Experiments such as quantum computation, precision measurements require a system that has very little noise[18][19][20]. Trapped ions is a great platform for these experiments as the system is very much isolated from its environment. Even though trapped ions are isolated from its environment, it can be interacted with radiation. The benefits of using a trapped ion system also include the ability to control the size of the system. As individual loading can be controlled this allows the user to specify exactly how big they want their system to be.

1.1 RF trap theory

Earnshaw's theorem tells us that a charged particle cannot be confined by a static electric field [2] [1]. There are two primary techniques for trapping ions. One is the Penning trap which utilizes static magnetic and electric fields and the other is the radio frequency (rf) Paul trap which uses alternating electric fields[21]. Although both different types of ion traps can trap ions, the ions in the Penning trap will be rotating at the cyclotron freqeuncy, which adds technical difficulties in manipulating the ions. As opposed to the Penning trap, rf Paul traps have localized ions that allow addressing each ion simpler. In this thesis, we will be focusing on rf Paul traps.

Assume a charged particle moving in one dimension with an external oscillating electric field $\vec{E}(x,t) = \vec{E}(x)\cos(\Omega_{rf}t)$, where Ω_{rf} is the angular driving frequency of the external field. The equation of motion is

$$m\ddot{x}(t) = \vec{F}(t) = e\vec{E}(x)\cos(\Omega_{\text{rf}}t) \tag{1.1}$$

If $\vec{E}(x)$ is spacially homogeneous, then $\ddot{x} = \frac{e}{m}E_0\cos(\Omega_{\text{rf}}t)$, resulting in harmonic motion $x(t) = -\frac{eE_0}{m\Omega_{\text{rf}}^2}\cos(\Omega_{\text{rf}}t)$. The time-averaged force over one period on the particle will hence be 0 and there is no net confinement as the time-averaged force is independent of x.

To create an effective confining potential, a field gradient can be introduced ($\frac{\partial E}{\partial x} \neq 0$).

$$\ddot{x}(t) = \frac{e}{m}\vec{E}(x)\cos(\Omega_{\text{rf}}t) \tag{1.2}$$

$$x(t) = x_0(t) + x_1(t) \tag{1.3}$$

We have seperated the particle's motion into two pieces, $x_0(t)$ exhibits large displacements with slow oscillations and $x_1(t)$ exhibits small displacements with fast oscillations. We will see that the slow frequency associated with $x_0(t)$ will be roughly 10 times slower than the fast frequency associated with $x_1(t)$. The motion of $x_1(t)$ will have frequency that is equal to the rf driving frequency.

Plugging equation 1.3 back into 1.2

$$\ddot{x_0} + \ddot{x_1} = \frac{e}{m}\vec{E}(x_0 + x_1)\cos(\Omega_{\text{rf}}t) \tag{1.4}$$

Taylor expanding the electric field to 1st order since this includes the field gradient,

$$\ddot{x_0} + \ddot{x_1} = \frac{e}{m}\left(\vec{E}(x_0) + \frac{\partial E(x_0)}{\partial x}x_1\right)\cos(\Omega_{\text{rf}}t) \tag{1.5}$$

As previously assumed that $\dot{x}_1(t) \gg \dot{x}_0(t)$, this leads to $\ddot{x_1} \gg \ddot{x_0}$. The assumption that $x_1(t) \gg x_0(t)$ also leads to $\vec{E} \gg \frac{\partial E(x_0)}{\partial x}x_1$

The combination of these approximations results in,

$$\begin{aligned} \ddot{x_1}(t) &= \vec{E}(x_0)\cos(\Omega_{\text{rf}}t) \\ x_1(t) &= -\frac{E(x_0)}{\Omega_{\text{rf}}^2}\cos(\Omega_{\text{rf}}t) \end{aligned} \tag{1.6}$$

Now we can plug equation 1.6 back into equation 1.2 and average over a period of the rf drive to get the net force

$$\left\langle \ddot{x_0} + E(x_0)\cos(\Omega_{\rm rf}t) = \left(E(x_0) - \frac{\partial E(x_0)}{\partial x}\frac{E(x_0)}{\Omega_{\rm rf}t}^2 \cos(\Omega_{\rm rf}t) \right)\cos(\Omega_{\rm rf}t) \right\rangle_T$$

$$\ddot{x_0}(t) = -\frac{e^2}{4m\Omega_{\rm rf}^2}\frac{\partial}{\partial x}E^2(x_0) \tag{1.7}$$

$$\langle \vec{F} \rangle_T = m\ddot{x_0}(t) = -e\frac{\partial}{\partial x}\big(\frac{e}{4m\Omega_{\rm rf}^2}E^2(x_0)\big) \equiv -e\frac{\partial \Psi_p}{\partial x} \tag{1.8}$$

$\Psi_{\rm p}$ is the psuedopotential. It is an approximate conservative potential that the ion experiences on slow timescales associated with $x_0(t)$. We see that the time averaged force is non-zero and it drives the particle towards lower field. In this heuristic derivation, we assumed that the particle's motion is seperated into two parts, x_0 and x_1, large and small displacements respectively. In the later section, we will see that the x_1 motion corresponds to micromotion oscillating at the rf frequency and x_0 motion corresponds to the slower secular frequency which we are interested in. For the work described here, $\Psi_{\rm p}$ is harmonic and the oscillation frequency in this harmonic psuedopotential is known as the secular frequency.

1.1.1 Psuedopotential and secular frequency

We have seen that the electric field must not have a gradient term in order for trapping. The quadrapole potential gives rise to a gradient in the electric field. The symmetric term that provides a trapping potential is,

$$\Phi(x,y,z) = \big(\frac{x^2+y^2-2z^2}{2r_0^2}\big)V_0\cos(\Omega_{\rm rf}t) \tag{1.9}$$

Solving for the electric field,

$$\vec{E}(x,y,z) = -\vec{\nabla}\Phi = -\frac{V_0\cos(\Omega_{\rm rf}t)}{r_0^2}(x\hat{\mathbf{x}} + y\hat{\mathbf{y}} - 2z\hat{\mathbf{z}}) \tag{1.10}$$

Plugging the electric field into the time-averaged force from equation 1.8,

$$\langle\vec{F}(t)\rangle_T = -e\Big(\frac{\partial}{\partial x}(\frac{eV_0^2}{4m\Omega_{\rm rf}^2 r_0^4}x^2\hat{\mathbf{x}}) + \frac{\partial}{\partial y}(\frac{eV_0^2}{4m\Omega_{\rm rf}^2 r_0^4}y^2\hat{\mathbf{y}}) - \frac{\partial}{\partial z}(\frac{eV_0^2}{4m\Omega_{\rm rf}^2 r_0^4}2z^2\hat{\mathbf{z}})\Big) \tag{1.11}$$

which gives the following equations of motion

$$\begin{aligned}
\ddot{x} &= -\frac{e^2V_0^2}{2m^2\Omega_{\rm rf}^2 r_0^4}x \\
\ddot{y} &= -\frac{e^2V_0^2}{2m^2\Omega_{\rm rf}^2 r_0^4}y \\
\ddot{z} &= -2\frac{e^2V_0^2}{2m^2\Omega_{\rm rf}^2 r_0^4}z
\end{aligned} \tag{1.12}$$

From which we immediately recognize as the harmonic oscillaion frequencies

$$\omega_{x,y,secular} = \frac{eV_0}{\sqrt{2}m\Omega_{\rm rf}r_0^2} \qquad \omega_{z,secular} = -\frac{2eV_0}{\sqrt{2}m\Omega_{\rm rf}r_0^2} \tag{1.13}$$

1.1.2 Mathieu Equation

In the previous sections, we have averaged out the fast oscillation that the particle experiences and derived the formula for the secular frequency. Now, let us look at the full solution to our particle and oscillating electric

field. Starting from the equation of motion, and potential of the form from equation 1.9,

$$\begin{aligned} m\ddot{x} &= -\frac{eV_0}{r_0^2}\cos(\Omega_{\mathrm{rf}}t)x \\ \ddot{x} + \frac{eV_0}{mr_0^2}\cos(\Omega_{\mathrm{rf}}t)x &= 0 \end{aligned} \tag{1.14}$$

We can add the effect of a static uniform DC potential,

$$\ddot{x} + \frac{e}{mr_0^2}(U + V_0\cos(\Omega_{\mathrm{rf}}t)x) = 0 \tag{1.15}$$

Following the standard procedure to cast this in Mathieu equatoin form, we define the parameters a_{x}, q_{x} and τ:

$$a_x = \frac{4eU}{m\Omega_{\mathrm{rf}}^2 r_0^2} \qquad\qquad q_x = -\frac{2eV_0}{mr_0^2\Omega_{\mathrm{rf}}^2} \tag{1.16}$$

$$\frac{d^2x}{d\tau^2} + 2q_x\cos(2\tau)x = 0 \tag{1.17}$$

Where $\tau = \frac{\Omega_{\mathrm{rf}}t}{2}$. Equation 1.17 is known as the Mathieu equation. The general solution is

$$x_k(\tau) = A_k e^{\mu_k\tau}\sum_{n=-\infty}^{\infty} C_{n,k}e^{2in\tau} + B_k e^{-\mu_k\tau}\sum_{n=-\infty}^{\infty} C_{n,k}e^{-2in\tau} \tag{1.18}$$

with

$$\mu_k = \alpha_k \pm i\beta_k$$

A_k and B_k are integration constants whose values depend on the initial conditions of the ions. The constants $C_{n,k}$ depend on parameters a and q. $C_{n,k}$ can be solved by plugging in the solution back into 1.17 and obtaining a recursion relation. It can be followed in [12].

In order for our particle to be bounded and stable, $\alpha_k = 0$, or else μ_k will have an exponential term instead of an oscillatory term. If $\beta_k =$ integer, the motion will be periodic but unstable. The first order solution is

$$x(t) \approx x_0 \cos(\omega_{sec} t)\big[1 - \frac{q}{2}\cos(\Omega_{\mathrm{rf}} t)\big] \tag{1.19}$$

with the definitions

$$\beta = \sqrt{\frac{q^2}{2} + a} \tag{1.20}$$

$$\omega_{sec} = \frac{\beta \Omega_{\mathrm{rf}}}{2} \tag{1.21}$$

The result is that along with the secular frequency, the particle also oscillates at a much smaller amplitude at the rf frequency. The motion at the rf frequency is known as micromotion. The following position vs time plot shows the typical oscillatory behavior of an ion.

The stability of the particle's trajectory depends on the values of a and q. The region $0 < \beta_{r,z} < 1$ is the section that we can trap ions as shown in figure 1.2. The boundaries of the stability region is when $\beta \neq$ integer. This can be seen from equation 1.21 that if $\beta =$ integer, then the secular

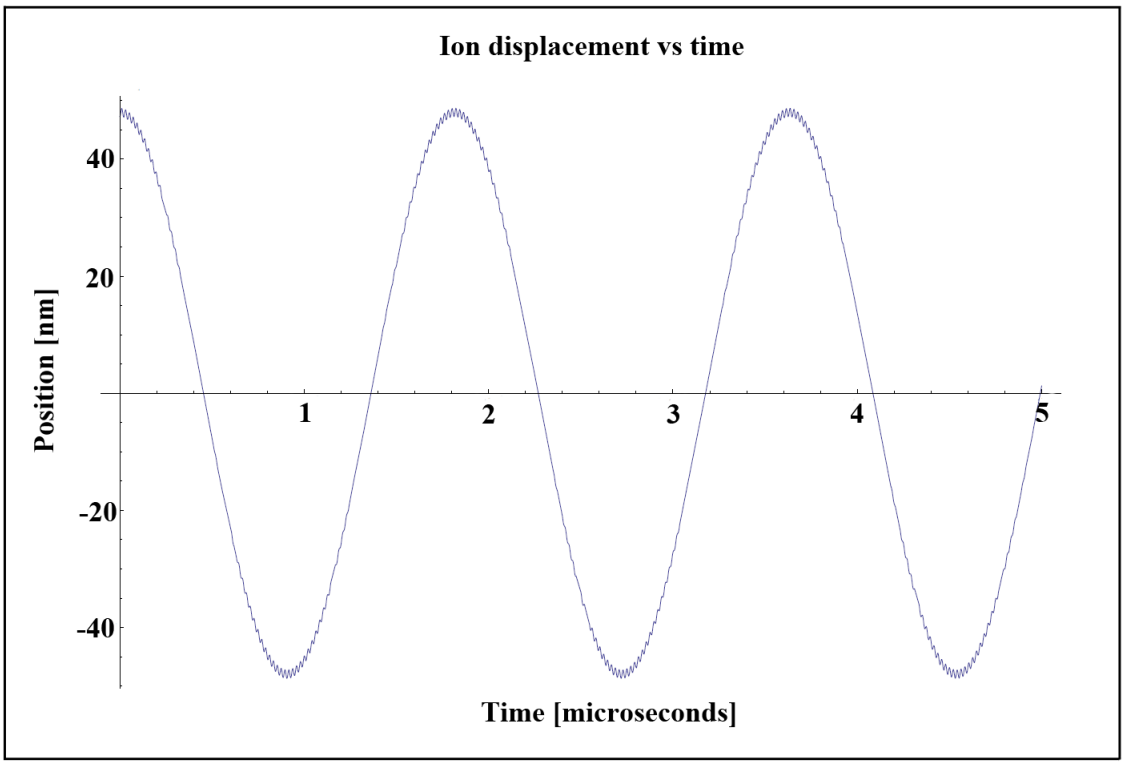

Figure 1.1: Secular motion and micromotion plotted. The amplitude of the micromotion is about 1 % of the secular motion amplitude. U = 1V, m = 174 amu, $V_0 = 630$ V, $\Omega_{\rm rf} = 2\pi \times 48$ MHz, $r_0 = 512$ μm

frequency will be a harmonic of the RF frequency, which would then lead to parametric resonance and drive the ion out of the trap. There exists higher order stability regions, but ion traps typically work in the 1st stable region as a large q would violate the psuedopotential approximation [22].

1.2 Vacuum requirements

In order to obtain long trapping times, low background gas collisions with our ions is necessary. Our chamber is under ultra-high vacuum environment ($\sim 10^{-11}$ Torr) which corresponds to roughly a few collisions per hour. Each experiment typically runs for about a few ms and repeated many

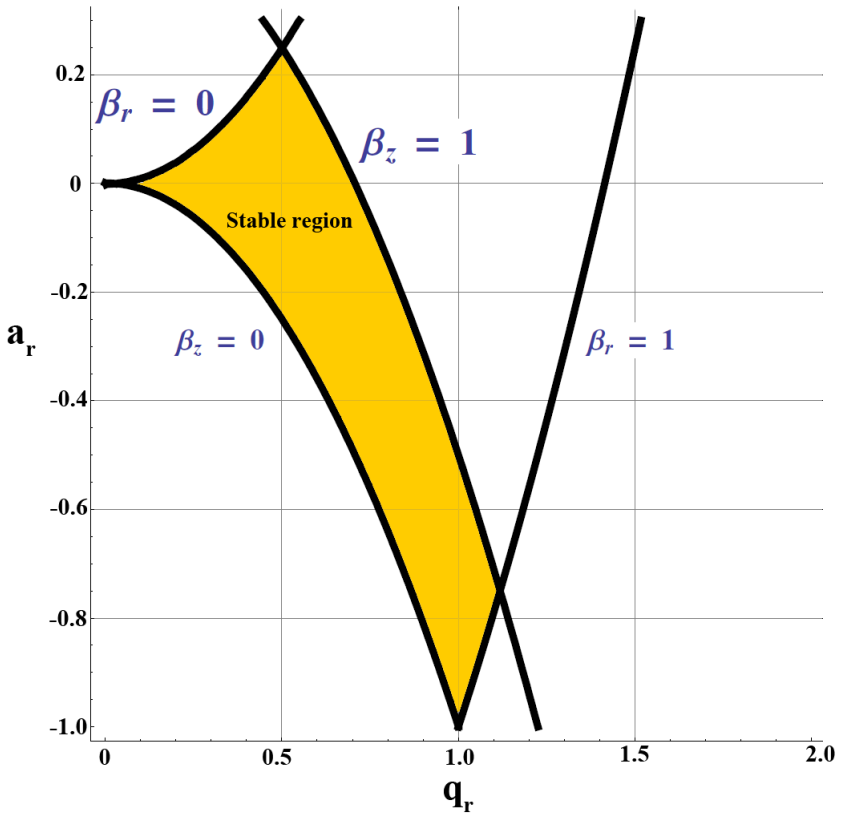

Figure 1.2: Mathieu stability diagram. Yellow region corresponds to the 1st stable region and periodic region. Our experiment typically operates around $\beta_z \approx 0.02$ and $\beta_r \approx 0.17$

times[19]. This lifetime would mean that the experiment would not notice the decoherence from background collisions. The average lifetime of our ions are on the order of 30 minutes, where the limitation is likely due to glancing background collisions driving the Yb ions into the F state.

1.2.1 Chamber assembly

The vacuum chamber used is a 6 inch stainless steel octogon. ConFlat flanges are used to seal all components as baking the chamber is required to outgas any water left on the inner surface of the chamber. Each component is cleaned in an ultrasonicator with distilled water and methanol before assembling. Once the parts are cleaned, the entire system is assembled with extreme care to make sure no dust or foreign objects fall into the chamber. Care is also taken with tightening up the ConFlat flanges as leaks can occur if the copper gasket does not sit evenly with the flange. There are different methods to tightening up ConFlat flanges, but the method which was used on this chamber was such that a 50 μm gap is left between any mating parts. A feeler gauge was used to measure the gap in between the CF flanges. The gap is left to allow any adjustments to tighten up the gasket if there is a leak detected at any point in time. After sealing up the entire chamber, the chamber is pumped out with a turbomolecular pump attached to the UHV angle valve. Once the pressure flattens out at around 10^{-8} Torr, the entire assembly is moved into an oven where we bake anywhere from 2 weeks to 1 month at 200 degrees C. The limitation to the temperature at which we set at is due to the glass to metal seal as it can get softened at high temperatures. The background gas in the chamber is monitored with an RGA to identify when the partial pressure for water has effectively stop dropping. A typical RGA scan can be seen in Figure 1.3

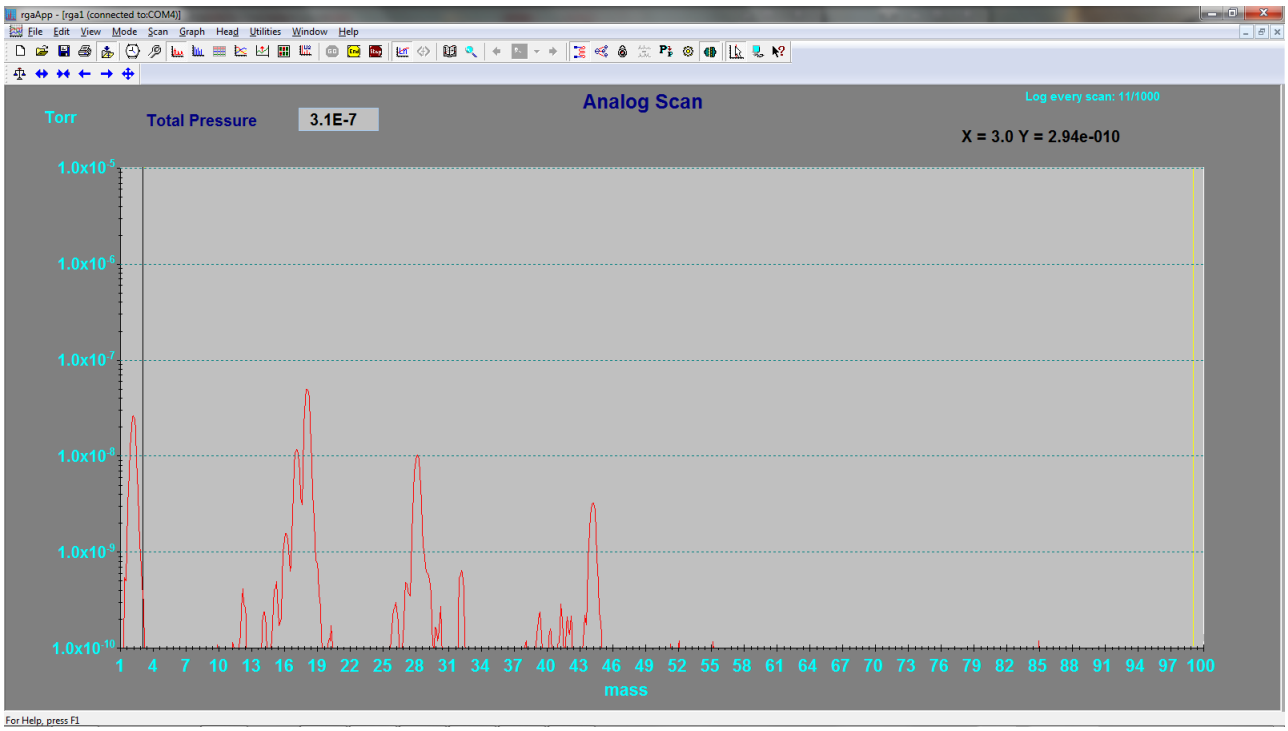

Figure 1.3: Typical RGA scan during bakeout. The dominant peak is around 16 AMU, which corresponds to water inside the chamber. The RGA scan helps us determine how long of a bakeout we should go on for. As the bakeout's primary purpose is to get rid of the water inside the chamber. Typically, if the water level hasn't changed over a day or so, we slowly ramp the chamber back to room temperature.

The different pumps used in evacuating the gas load includes a 40 L/s ion pump, titanium sublimation pump and a nonevaporable getter. All three of these pumps work as passive pumps, as it waits for a particle to come into contact with it's surface and it sticks to the surface of that pump. The TiSub works by running 50A of current through a titanium filament and coats the surrounding surface that the filament sees. Multiple firings of the TiSub is needed in order to bring the pressure down, as the titanium surface of the nipple gets coated with background gas. Typically, an order of magnitude of pressure is reduced after finishing firing the Tisub. The

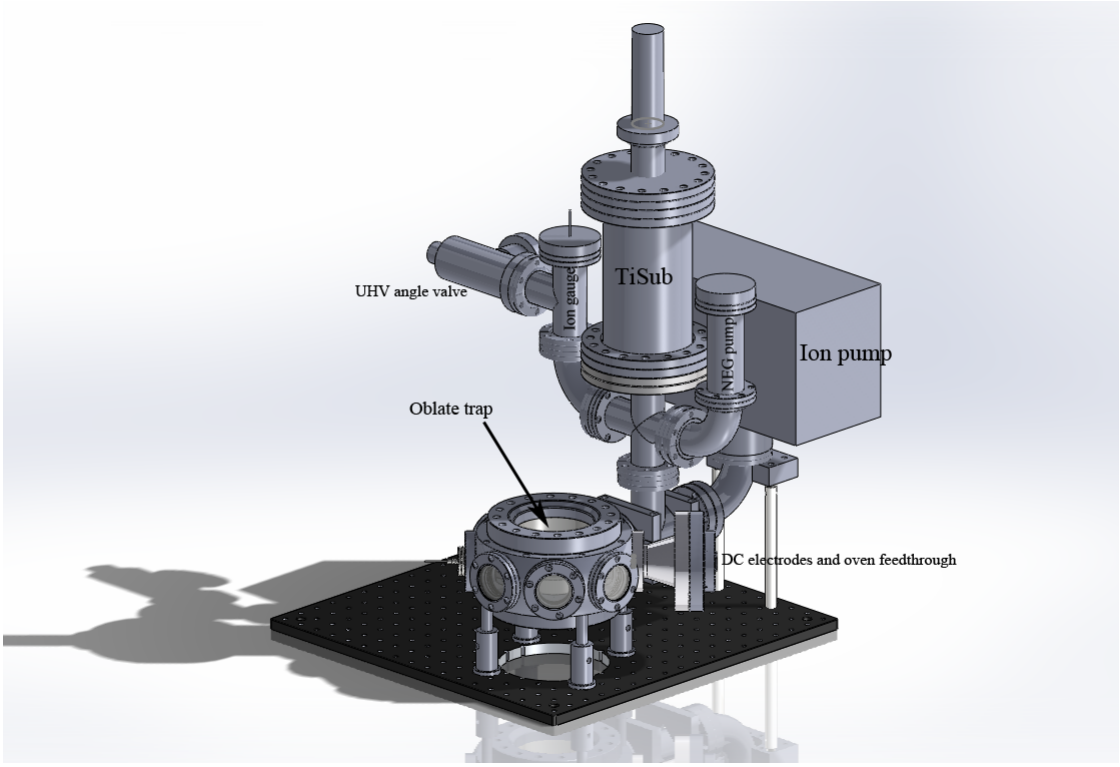

Figure 1.4: Vacuum assembly. The trap sits at the center of the octagon chamber. Custom reentrant viewports(2.69" diameter glass) sandwich the trap from above and below. The distance from the top (bottom) surface of the trap to the top (bottom) window is about 5.5 mm. There are a total of 5 2.75" Conflat flange viewports along the sides for optical access. The RF connection is opposite to the DC electrode connections. The TiSub is placed at a location such that the trap or any sensitive electronics does not have a line of sight to the titanium filament. So that there will be no coating of titanium on parts that we do not want to coat.

ion pump works by creating a high voltage (7 kV) to generate a plasma. Along with a strong magnetic field, this plasma is trapped in a region. When a background molecule comes into this region, the electrons ionize the gas molecule and strikes it to the cathode plate. Nonevaporable getter works by having an extremely porous surface which allows sorption process to occur. Once the getter is activated by running a high current, it begins to act as a passive pump. The NEG can be regenerated by reheating the pump, as the molecules stuck to the surface will be absorbed into the bulk.

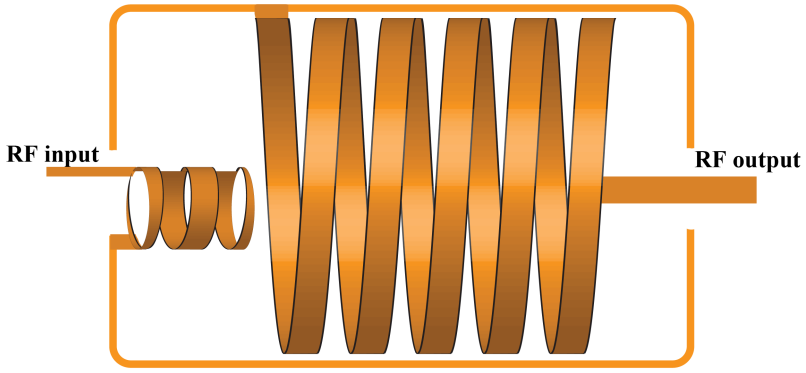

Figure 1.5: The helical resonator is designed to step up the input voltage and also match the impedance of the trap.

1.2.2 RF voltage

Another key part to trapping ions is the ability to deliver RF frequency at high voltage to the trap. It is difficult to find commercial electronics in this regime and hence we need to build a helical resonator to deliver the voltage. The helical resonator is a quarter wave resonator intended to step up the input voltage and match the impedance of the trap. The output impedence of our RF frequency source is at 50Ω while the trap impedence is not. The helical resonator solves this issue by adjusting the antenna of the pickup coil.

1.3 Oblate Paul trap

The trap used in this thesis is not a traditional 4 rod trap but rather an oblate Paul trap. The choice of this design was to optimize for photon collection and ease of assembly. Figure 1 shows the geometry of the trap. There are 3 regions to this trap; the DC connections, trapping region, and the RF connection. The entire trap is a 1 mm thick monolithic piece of

fused silica coated with a 20 nm base layer of titanium followed by 500 nm of gold. The trapping region is centered in a tapered section which transitions from 1 mm thickness to 140 μm for the RF ring. The RF connection has a gold trace which runs along the top surface of trap and forms the RF ring in the center 500 μm diameter cutout hole. Laser ablated gaps range from 30 μm (between RF ring and DC electrodes) to 200 μm (DC electrode gap far away from center). There are a total of 8 trenches which tunnel from the side of the trap and through the center of the trapping region. Each tunnel tapers from 250 μm entrance hole (at the edge) to 100 μm hole to the center of the trap. Six of the tunnels are used to send various laser light into to our ions. One of the holes is used for sending our neutral Yb atoms to the trapping region and opposite of that hole is the atom dump port. The tapering of the holes is designed so that the Rayleigh range of our most red (935 nm) beam would clear the trap without clipping.

1.3.1 Optical access

Photon collection efficiency is an important factor as we would like to collect as much of the ion fluorescence as possible. Ideally, we would have a 4π coverage, but this is not possible as you need to have electrodes to form the trap as well. Therefore having a thin profile and sending our laser beams through the trenches allows us to collect photons from the top and bottom without any obstruction. The overall fraction of the solid angle which we can collect light from is 0.72. With Fresnel losses from the fused silica viewports, the theoretical fraction of light that can be collected comes out to be 0.66. The distance between the inner surface of the top viewport to the top of the trap is about 11 mm.

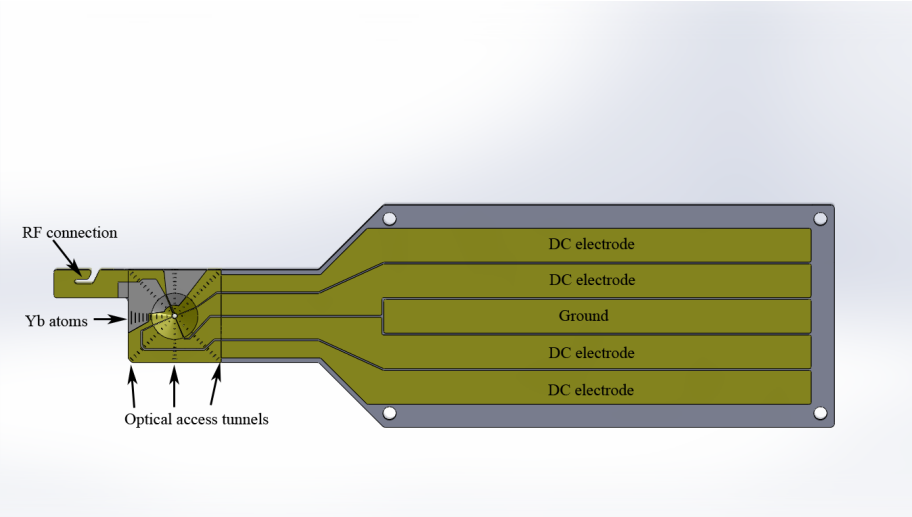

(a) The entire structure of the trap is a monolitic piece of fused silica glass. It is cut by Translume's laser ablation technology. Not pictured is the chip holder that holds the chip in place. The RF connection is designed to be a hook that latches onto a piece of beryllium copper metal. Once the chip is held in place by the chip holder, the beryllium copper metal tugs onto the RF connection spot. The springiness of the beryllium copper in theory provides the tension needed to make the connection secure.

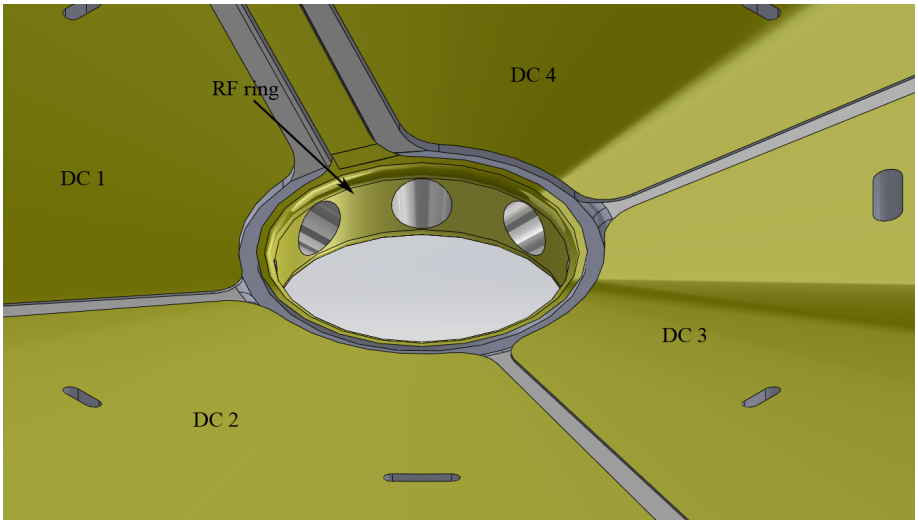

(b) The trapping electrodes are shown above with a total of 8 DC electrodes (top and bottom), and the RF ring that circumscribes the trapping region. For optical access, there are 6 trenches that each has an opening of 120 μm in diameter. The diameter of the trapping region is 500 μm

Figure 1.6

1.3.2 Simulation of trapping potential

Since our trap is not a perfect hyperbolic trap, we must find what the characteristic length (r_0) by simulating the potential via Comsol[23]. From the previous chapter, our potential takes the form

$$\Phi(x, y, z) = \frac{\Phi_0}{r_0^2}(x^2 + y^2 - 2z^2) \tag{1.22}$$

This leads to

$$E^2(x, y, z) = \frac{4\Phi_0^2}{r_0^4}(x^2 + y^2 + 4z^2) \tag{1.23}$$

By setting $\Phi_0 = 1V$ on the RF ring, while the voltage on the DC electrodes are all set to zero, a numerical solution for $E^2(x, y, z)$ was obtained, and the equation

$$E^2(x, y, z) = a(x^2 + y^2 + z^2) \tag{1.24}$$

was fitted to the data. The characteristic length is found to be $r_0 = 512$ μm.

1.3.3 Voltage breakdown test

Voltage breakdown tests were performed to determine electrode gap size, shape, etc. Three types of samples were tested: stencil mask deposited electrode, T-slotted electrode gaps and laser ablated gaps.

The stencil mask electrodes are made with 2 layers, an initial layer of 20 nm Titanium followed by 500 nm of gold. Various gap size were tested: 200 μm, 100 μm and 50 μm. Two gap sizes were tested for the inverted T-slots: 10 μm and 20 μm.

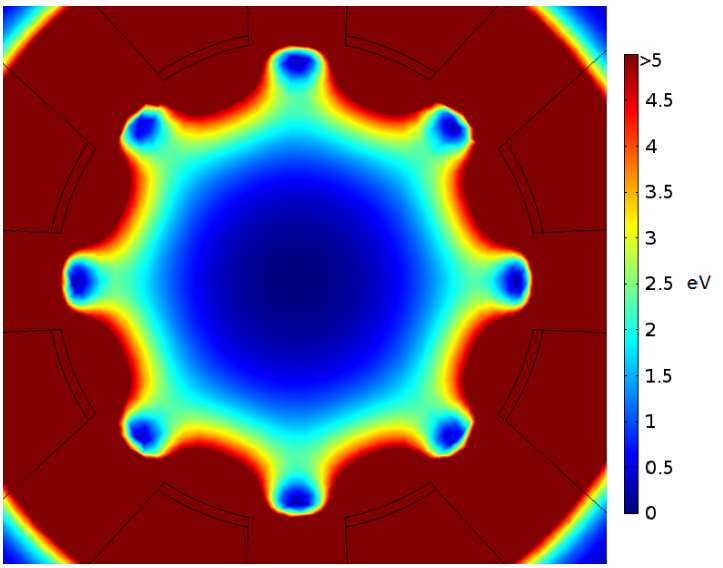

(a) Top view of trap

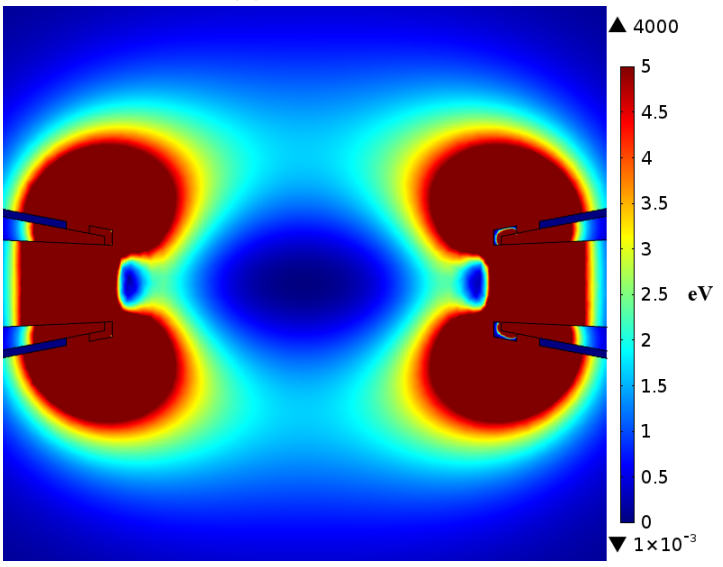

(b) Sideview of trap

Figure 1.7: Numerical results for pseudopotential produced by applying 500 V RF, 35 MHz RF frequency. Top and bottom DC electrodes are grounded. The well depth near the center of the trap is 1.6 eV. [23]

All of the stencil mask electrodes withstood 450 V of RF and 1.1 kV of DC voltage. For the inverted T electrodes, the breakdown voltages ranged from 100 to 300 V RF and 200 to 500 V DC. The laser ablated gaps, the breakdown voltages ranged from 340 to 680 V.

Figure 1.8

(a) Stencil mask (b) inverted T-slots (c) Laser ablated gaps

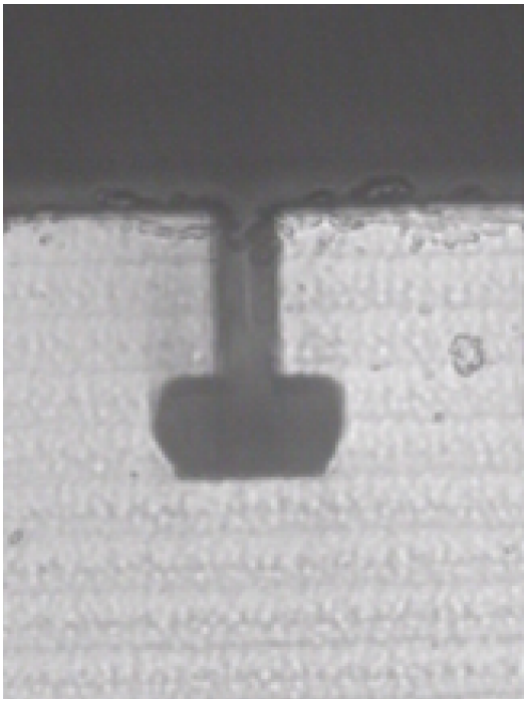

Figure 1.9: Side profile of inverted T-slots

1.3.4 Trap assembly

The trap is designed to be clamped in space by a chip carrier. With a 12 pin feedthrough, 10 of the feedthroughs connect to a machined piece of Macor with holes drilled designed to connect to copper wires. Fuzz buttons (wounded up thin strands of BeCu) are attached to each end of the copper wire inside the carrier. The Fuzz buttons act as springs to make sure that

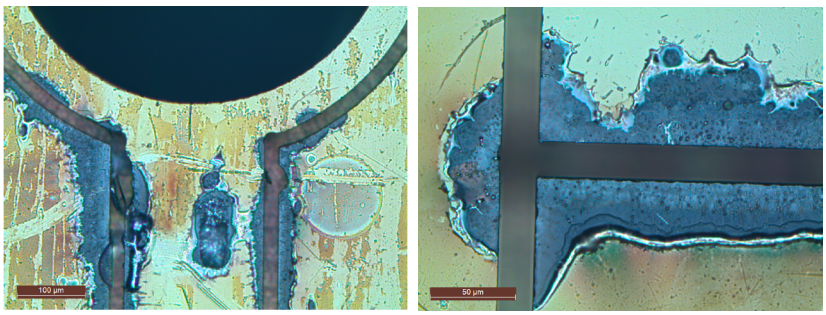

(a) (b)

Figure 1.10: typical damage for T-slots

when the clam shell carrier tightens up, each of the DC connections are still connected. Once the trap is in place, electrical continuity check is performed on all 10 connections. The RF connection is attached on the opposite side of the trap with a strand of BeCu that acts as a hook to latch onto the trap. The Yb oven is connected to one of the 12 pin feedthroughs and aligned to the oven port of the trap. The setup can be seen in figure 1.11

1.4 Doppler cooling

Although the ion is trapped in space, the kinetic energy of the ion is still very high ($\sim 1eV$). Therefore we must reduce it's motional energy before we can manipulate the internal states with better control. Doppler cooling is typically the 1st step in laser cooling any atomic species[3][25][24]. Doppler cooling works by exerting an optical force onto the atom, and by spontaneous emission from the excited state, it removes entropy from the atom and lowers the temperature of the atom. The states which we are adressing are typically electronic states with optical frequencies. Before we look at how Doppler cooling works for a trapped ion, it is instructive to look at a neutral atom with counterpropagating beams acting upon the

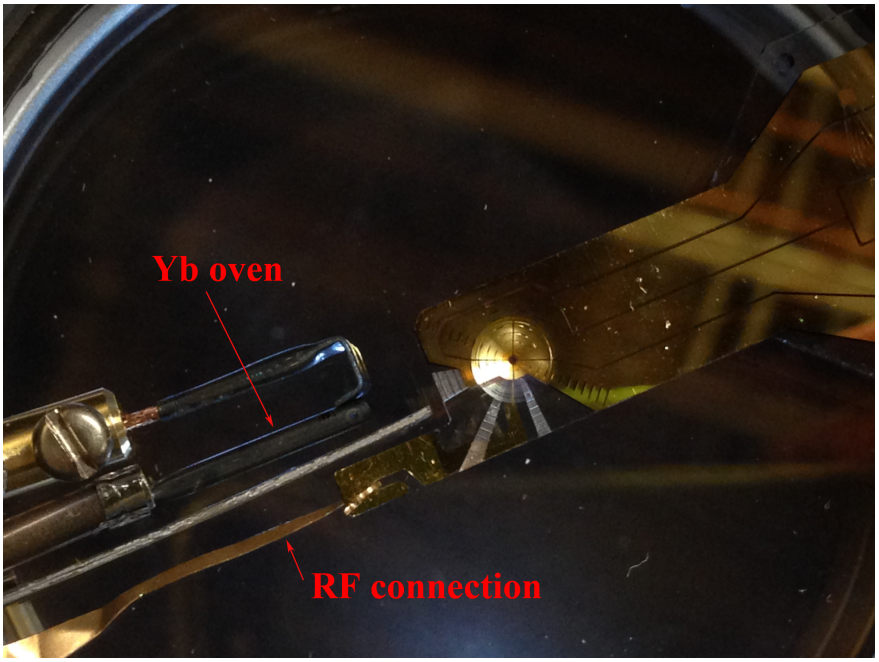

Figure 1.11: The Yb oven is made by packing small pieces of Yb foil down a stainless steel tube. The tube is then crimped on one end and spot welded to a bigger piece of stainless steel tube for structural support. The opening end of the Yb oven is spot welded as close as possible to to the tip as cold spots might occur which could lead to clogging of the oven. The RF is connected by a piece of BeCu metal. The elasticity of the metal acts as a spring that latches onto the trap.

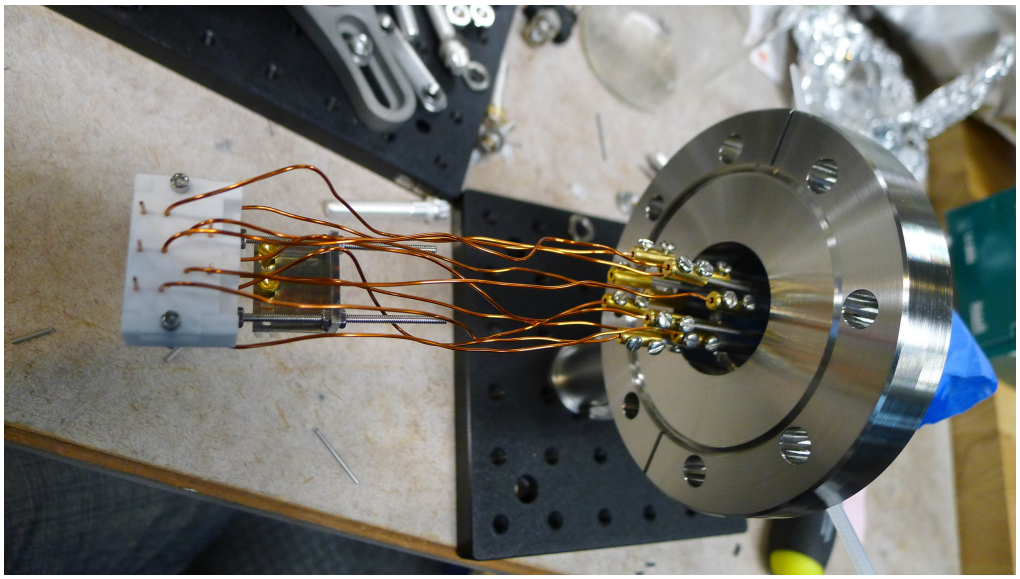

(a)

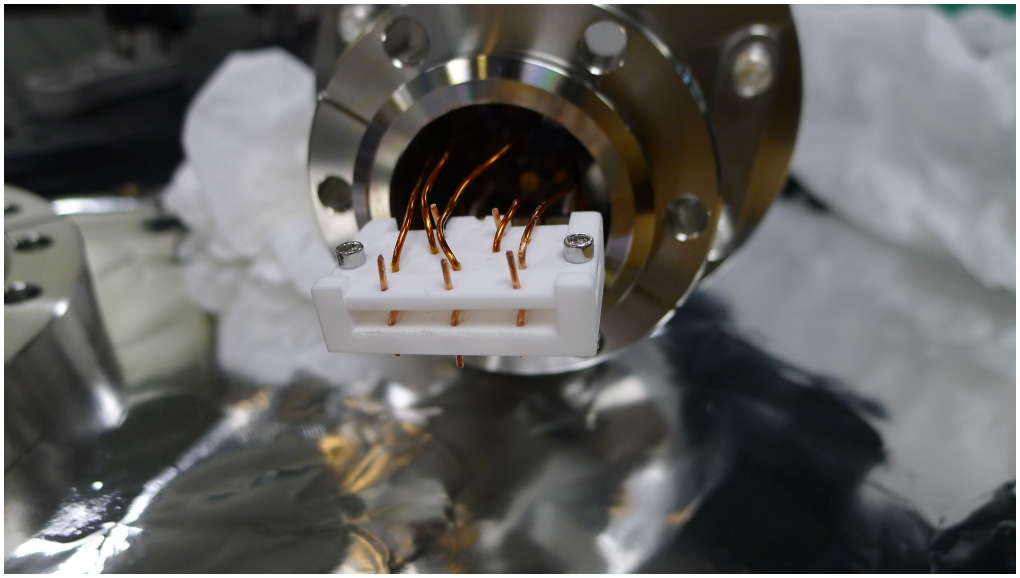

(b) The trap carrier is machined out of Macor. The design is to weave the copper wires into this clamshell and sandwich the trap in between the carrier. There are Fuzz Buttons attached to each copper wire inside the clamshell to make sure all 8 electrodes are electrically connected. Tightening the two screws pictured, the holder securely makes a connection with all the 8 DC electrodes.

Figure 1.12

atom. Let us assume the atom has only 2 states $|g\rangle$ and $|e\rangle$, ground and excited state of the atom with an energy difference of $E_{atom} = \hbar\omega_{\rm eg}$. The population of the excited state is given by

$$\rho_{\rm ee} = \frac{s_0}{2}\frac{1}{1+s_0+(2\delta/\gamma)^2} \tag{1.25}$$

where s_0 is the saturation parameter given by I/I_{sat}, δ is the laser detuning, $\delta = \omega_{\rm eg} - \omega_{\rm laser}$, and $\tau = 1/\gamma$ is the radiative lifetime of the excited state. I is the intensity of the laser and $I_{\rm sat} = \frac{\pi hc}{3\lambda^2\tau}$.

The scattering force of the photon onto the atom is given by

$$\vec{F}_{\rm scatt} = (photon\, momentum) \;\times\; (scattering\, rate) \tag{1.26}$$

We denote F_+ as the scattering force by the photons moving towards the right and F_- as the scattering force towards the left.

$$\vec{F}_{\pm} = \pm\frac{\hbar\vec{k}\gamma}{2}\frac{s_0}{1+s_0+(\frac{2(\delta\mp|\omega_D|)}{\gamma})^2} \tag{1.27}$$

Where $\omega_D = \vec{k}\cdot\vec{v}$ is the Doppler shift due to an atom moving with velocity $\vec{v}$. If we had two counterpropagating beams hitting the atom, the sum of the scattering force will be equal to

$$\vec{F}_+ + \vec{F}_- \approx \frac{8\hbar k^2\delta s_0\vec{v}}{\gamma(1+s_0+(2\delta/\gamma)^2)^2} \tag{1.28}$$

$$\vec{F}_{scatt} = -\beta\vec{v} \tag{1.29}$$

where $\omega_D = \vec{k}\cdot\vec{v}$ is the Doppler shift for an atom moving with velocity $\vec{v}$, and β is the damping coefficient. $\mathcal{O}((\omega_D/\gamma)^4)$ terms have been ignored.

Looking at equation 1.28, the scattering force will cool the particle to

zero velocity if there's no heating term, which is unphysical. The heating term arises from each spontaneous emission event, and corresponds to a kick of momentum in a random direction. The atom's kinetic energy after either an absorption or emission process is given by the recoil energy $E_r = \frac{\hbar^2 k^2}{2m} = \hbar\omega_r$. Hence, after both an absorption and emission event, the atom has gained $2E_r$ worth of energy. This happens at a rate of $2\gamma\rho_{ee}$ due to two beams. Equating the heating rate to the cooling rate

$$\vec{F}_{\text{scatt}} \cdot \vec{v} = 4\hbar\omega_r\gamma\rho_{ee} \tag{1.30}$$

Therefore,

$$\frac{8\hbar k^2 \delta s_0 \vec{v}}{\gamma(1 + s_0 + (2\delta/\gamma)^2)^2} = 4\hbar\omega_r\gamma\frac{s_0/2}{1 + s_0 + (2\delta/\gamma)^2} \tag{1.31}$$

we can solve for v from equation 1.31 to obtain

$$v^2 = \frac{\hbar\gamma^2}{8m\delta}(1 + (\frac{2\delta}{\gamma})^2) \tag{1.32}$$

Substituting v^2 into the kinetic energy term,

$$E_{\text{kinetic}} = \frac{1}{2}mv^2 = \frac{\hbar\gamma}{8}(\frac{2\delta}{\gamma} + \frac{\gamma}{2\delta}) \tag{1.33}$$

The minimum value of E_{kinetic} is when $\delta = -\frac{\gamma}{2}$. This is the optimal Doppler frequency for a given atom. Setting the minimum kinetic energy equal to $\frac{1}{2}k_bT$ results in the Doppler tempurature limit

$$\frac{1}{2}k_bT = \frac{\hbar\gamma}{8}(\frac{2\gamma/2}{\gamma} + \frac{\gamma}{2\gamma/2}) \tag{1.34}$$

$$T_{\text{Doppler}} = \frac{\hbar\gamma}{2k_b} \tag{1.35}$$

Following the same derivation as above, we can obtain similar results for a trapped ion being illuminated by a Doppler cooling beam. Instead of having counterpropagating beams, we only need a single Doppler cooling beam to cool. The force exerted by one beam is given by equation 1.27 and the expansion up to $\mathcal{O}(v)$ is given by

$$\vec{F} = \frac{\hbar\vec{k}}{2}\frac{s_0}{1 + s_0 + (\frac{2(\delta \mp |\omega_{\text{D}}|)}{\gamma})^2} \tag{1.36}$$

$$\vec{F} \approx \frac{\hbar\vec{k}}{2}\frac{s_0}{1 + s_0 + \frac{4\delta^2}{\gamma^2}} + \frac{4\hbar k^2}{\gamma}\frac{s_0\delta}{(1 + s_0 + \frac{4\delta^2}{\gamma^2})^2}\vec{v} \tag{1.37}$$

Averaging over many oscillation periods, the cooling rate is hence,

$$\dot{E}_{\text{c}} = \langle\vec{F}\cdot\vec{v}\rangle = \frac{\hbar k}{2}\frac{s_0}{1 + s_0 + \frac{4\delta^2}{\gamma^2}}\langle v\rangle + \frac{4\hbar k^2}{\gamma}\frac{s_0\delta}{(1 + s_0 + \frac{4\delta^2}{\gamma^2})^2}\langle v^2\rangle \tag{1.38}$$

The term with $\langle v\rangle$ averages to 0 over many cycles. Which leaves us with only the term that has v^2. The heating rate is given by [11]

$$\dot{E}_{\mathrm{h}} = \dot{E}_{\mathrm{abs}} + \dot{E}_{\mathrm{em}} \tag{1.39}$$

$$= \dot{E}_{\mathrm{abs}}(1+\xi) \tag{1.40}$$

where $\xi = 2/5$ is a geometry factor that takes into account the dipole emission pattern. We plug the energy of each emission and the rate at which it occurs at to obtain

$$\dot{E}_{\mathrm{h}} = \frac{(\hbar k)^2}{2m} \frac{\gamma s_0}{1 + s_0 + \frac{4\delta^2}{\gamma^2}} (1+\xi) \tag{1.41}$$

Once again, we equate the heating rate to cooling rate,

$$\frac{(\hbar k)^2}{2m} \frac{\gamma s_0}{1 + s_0 + \frac{4\delta^2}{\gamma^2}} (1+\xi) = \frac{4\hbar k^2}{\gamma} \frac{s_0 \delta}{(1 + s_0 + \frac{4\delta^2}{\gamma^2})^2} \langle v^2 \rangle \tag{1.42}$$

Solving for $\langle v^2 \rangle$, we obtain

$$\langle v^2 \rangle = \frac{\hbar\gamma}{8}(1+\xi)(\frac{\gamma}{2\delta} + \frac{2\delta}{\gamma}) \tag{1.43}$$

Plugging this value into the average kinetic energy and equating it to $\frac{k_{\mathrm{B}}T}{2}$,

$$k_{\mathrm{B}}T = \frac{\hbar\gamma}{8}(1+\xi)(\frac{\gamma}{2\delta} + \frac{2\delta}{\gamma}) \tag{1.44}$$

The minimum temperature will be

$$T_{\min} = \frac{\hbar\gamma}{4k_{\mathrm{B}}}(1+\xi) \tag{1.45}$$

For typical laser coolable atoms or ions, this temperature is $\sim 1mK$.

1.5 Photoionization

There are multiple ways of generating Yb ions, such as laser ablation, electron bombardment and photoionization. Our method of generating ions is by phonotionization. This allows us to have better isotope selectivity and eliminates violent charging effects by methods such as laser ablation and electron bombardment. Placing small pieces of Yb foil into a stainless steel tube (inner diameter $\sim 1mm$) and running about 2-3 amps of current creates a jet of neutral Yb out of the oven. Neutral Yb fluorescence is detected by a PMT to ensure that there is Yb in our trapping region. Figure 1.15 shows the spectrum of the ${}^1S_0 \rightarrow {}^1P_1$ transition. 399 nm is then tuned to the isotope which we would like to load. Once the neutral Yb is in the ${}^1P_1$ state, 369 nm light will photoionize the atom to create singly ionized Yb^+.

1.6 Lasers

Loading and cooling Yb ions require a total of 3 lasers, 369 nm for laser cooling and driving Yb ions into the continuum, 399 nm for ${}^1S_0 \rightarrow {}^1P_1$ of neutral Yb, and 935 nm for repumping ${}^2D_{3/2} \rightarrow {}^3[3/2]_{1/2}$. For our 369 nm laser, we use a Moglabs 369 nm diode.

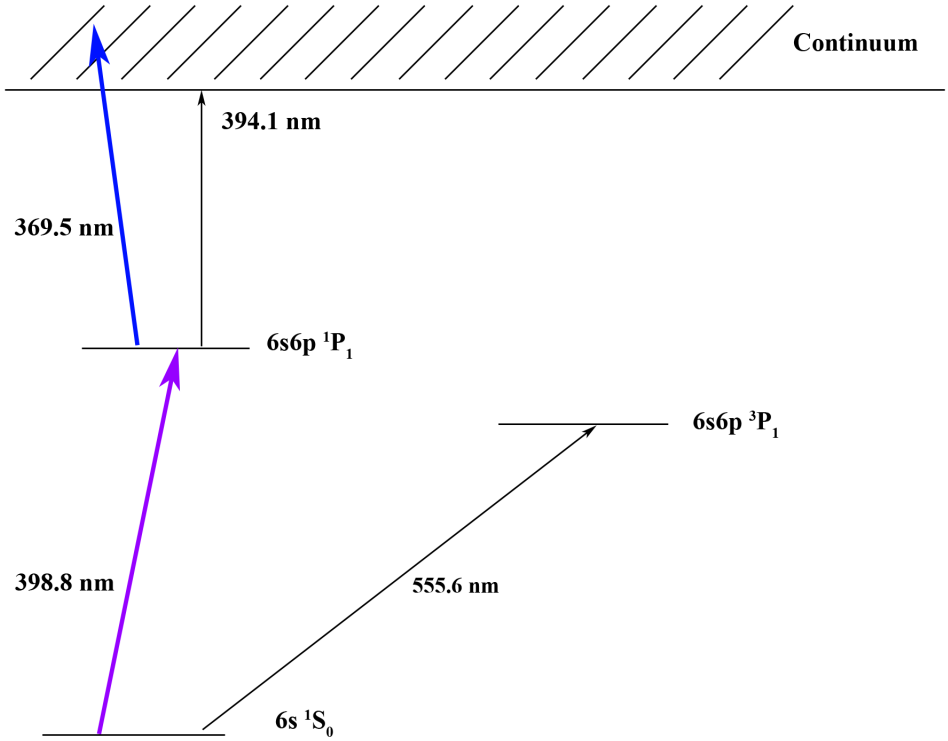

Figure 1.13: Energy diagram for neutral Yb. Values quoted from [5]. A 398.8 nm laser is used to drive $^1S_0$ to $^1P_1$ transition. Once the atom is in this state, 369.5 nm light drives the atom into the continuum, therefore ionizing the atom.

	Output power	Power at trap
Moglabs 369 nm diode	8mW	10 μW
Toptica 399 nm DL 100 Pro	30mW	60 μW
DBR 935 nm	30 mW	2 mW

Table 1.1: The 3rd column is the typical power needed for loading/cooling ions, as the optical power out of the laser can be split off however many ways necessary for other purposes such as wavemeter monitor, locks, etc

1.6.1 Laser stabilization

Frequency stability is a critical part to laser cool ions. As we want to sit $\gamma/2$ red detuned of the transition for the 369 nm light which happens to

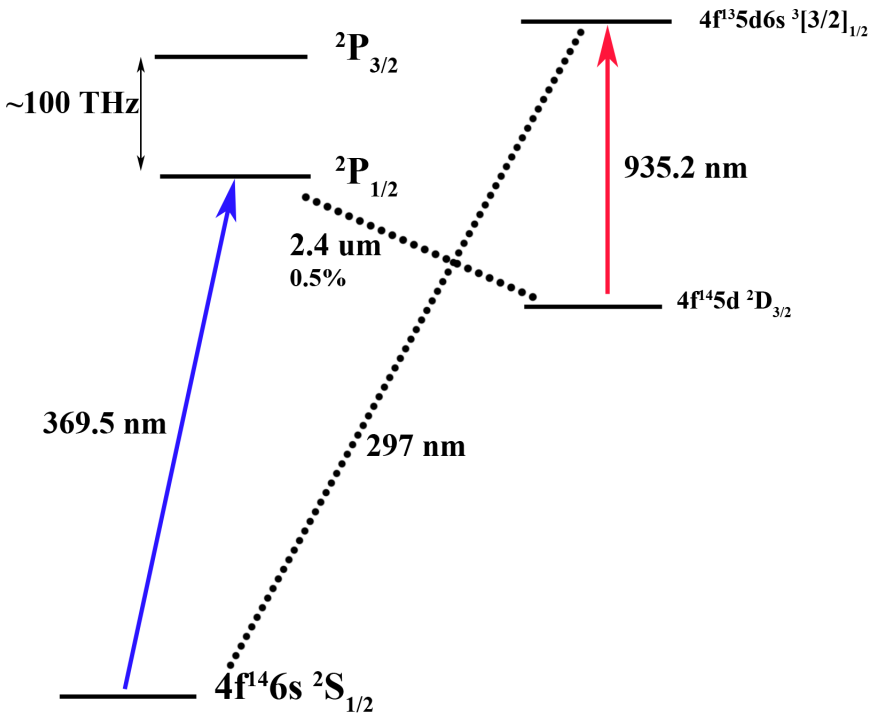

Figure 1.14: Energy diagram for Yb^+. Values quoted from [5]. The main Doppler cooling beam is centered around 369.5 nm. About 0.5% of the time, it falls from $^2P_{1/2}$ to the $^2D_{3/2}$ state. We clear this state by shining 935 nm light to repump it to the $^3[3/2]_{1/2}$ state which then falls back to our cycling transition starting at $^2S_{1/2}$.

be about 10 MHz red detuned, we require the stability of our laser to not drift for the duration of our experiments. Any blue detuned light will heat the ion out of the trap. We PDH lock the 369 nm laser to an optical cavity which has a free spectral range of 1.064 GHz. The 399 nm and 935 nm are software locked by the WSU2 wavemeter.

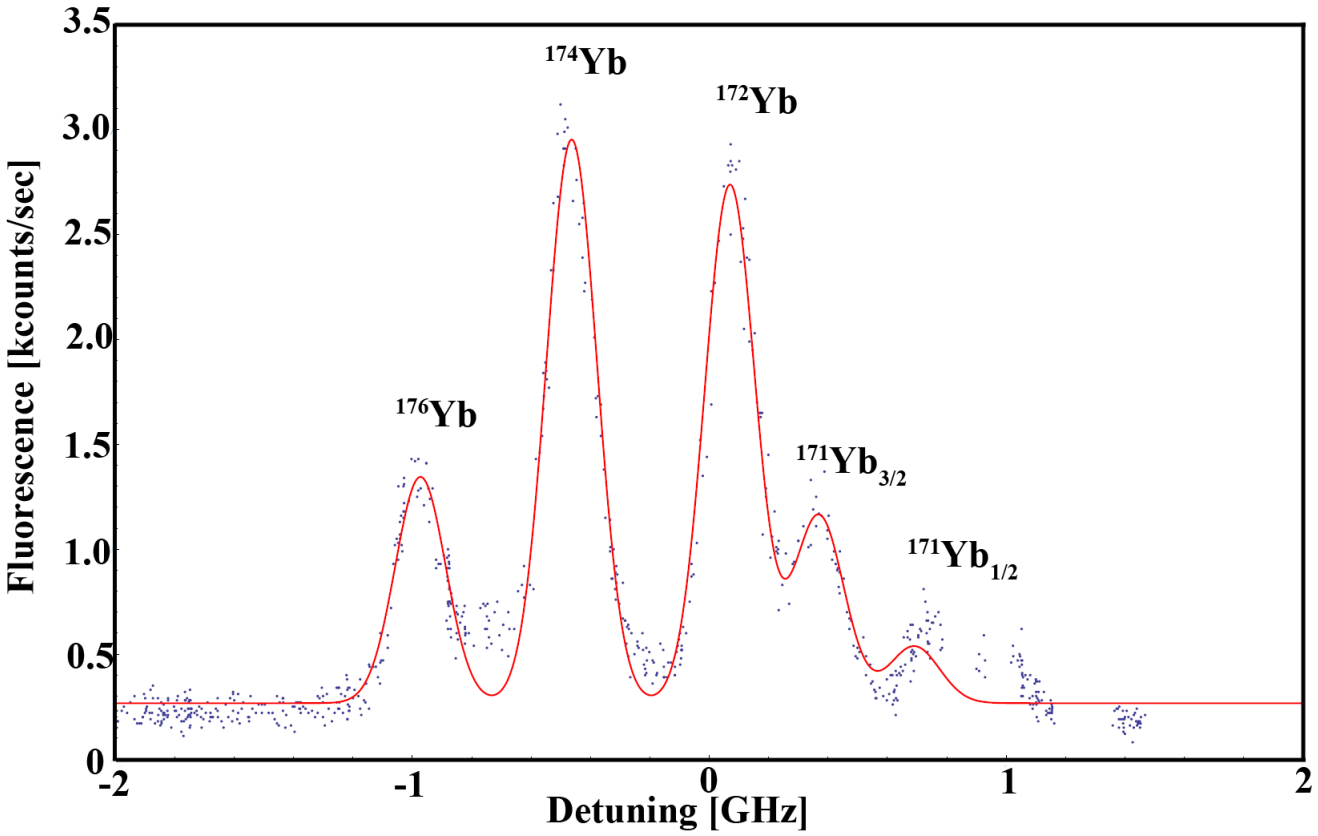

Figure 1.15: Neutral Yb spectrum of ${}^1S_0 \rightarrow {}^1P_1$. Center frequency is set to 751.526800 THz. Detecting fluorecence with PMT. Fit was calculated by allowing ^{174}Yb amplitude to vary, and keeping all the other amplitudes fixed relative to ^{174}Yb, since we have a natural abundance source. The odd isotopes have relative Clebsch-Gordon coefficients due to their hyperfine splitting.

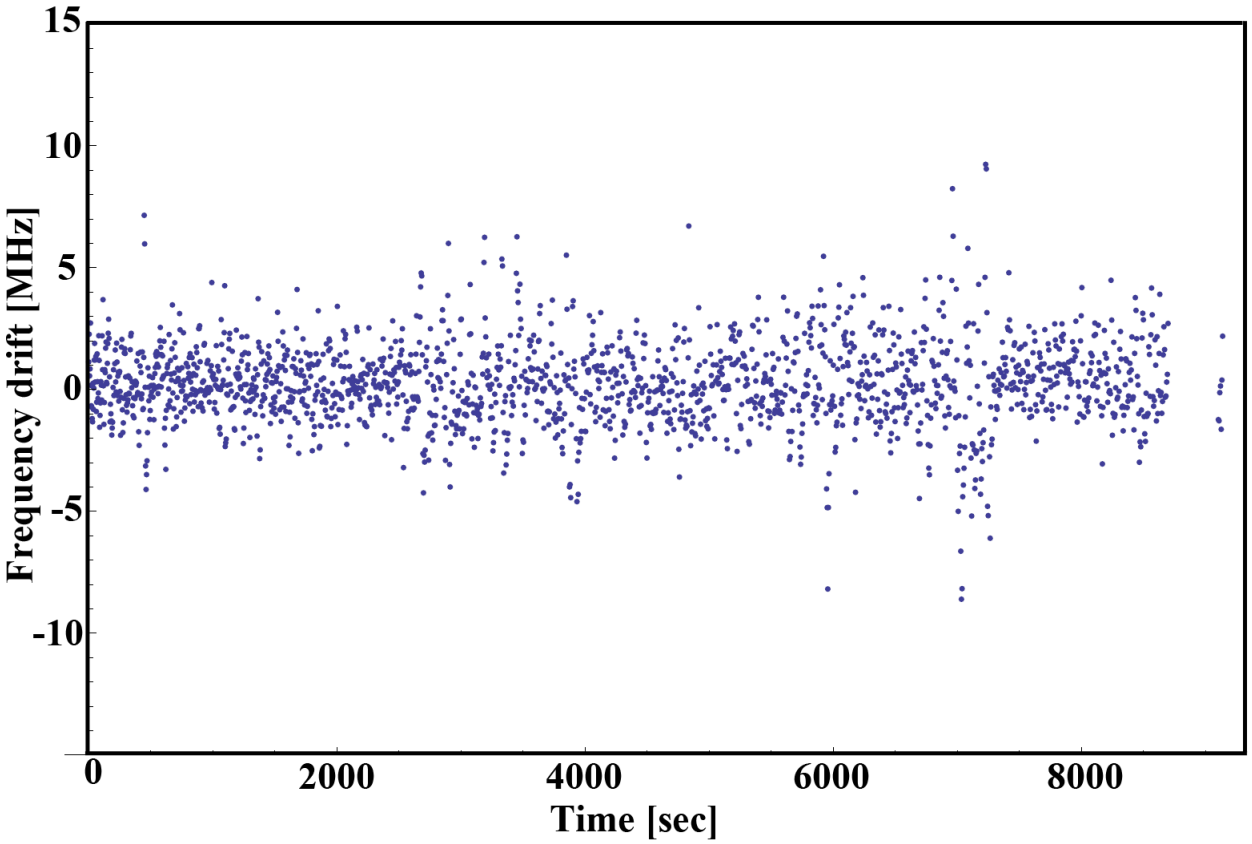

Figure 1.16: 935 software locked by wavemeter. The stability of the 935 nm repumper is not as crucial as our 369 nm Doppler cooling light, because we have enough power to power broaden the line. We typically have about a 2 mW of 935 nm light on the ion.

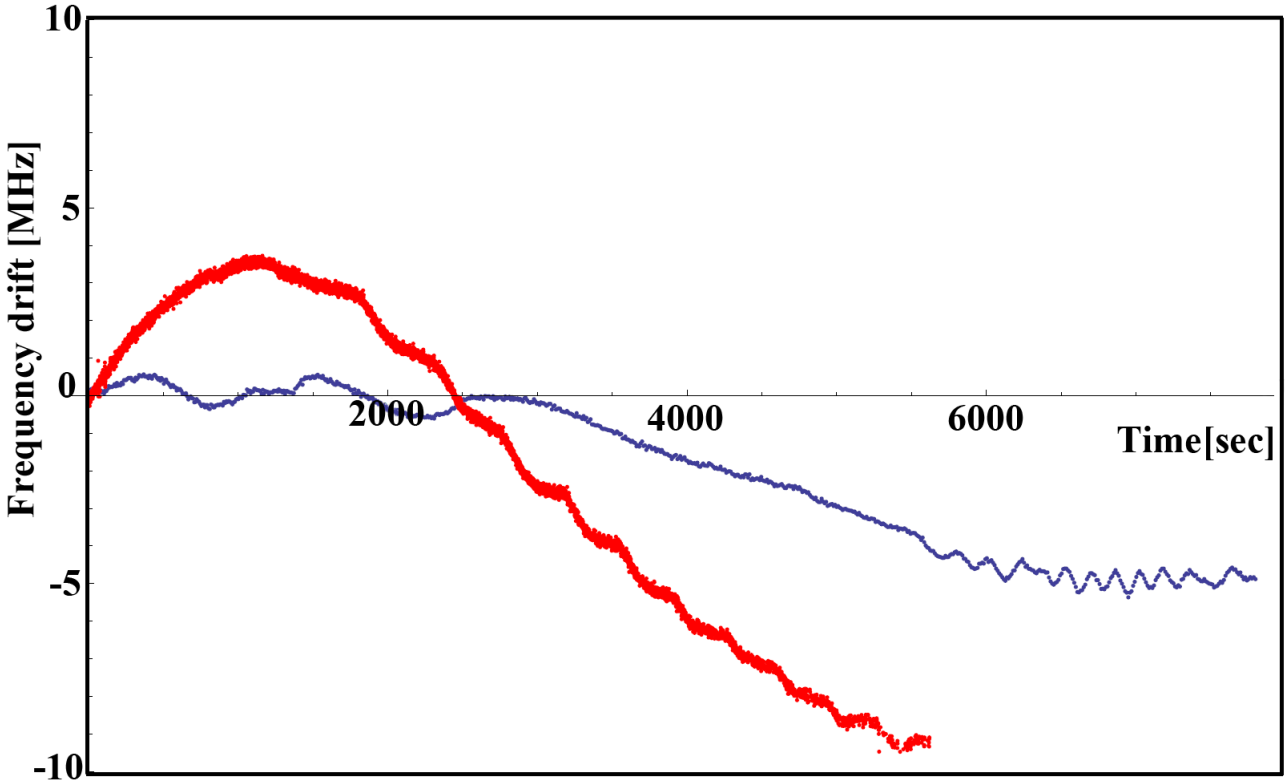

Figure 1.17: Both curves are monitoring the frequency drift of the 369 nm laser when it is locked to optical cavity. Red curve is before installing temperature stabilization. Blue curve is after installing temperature stabilization.

CHAPTER 2

Mode-locked laser interaction with single ion

2.1 Derivation of steady state scattering rate

The optical Bloch equations are given by [24][25]

$$\dot{\rho}_{ee} = -\gamma\rho_{ee} + \imath\frac{\Omega}{2}\rho_{ge} - \imath\frac{\Omega}{2}\rho_{eg} \tag{2.1}$$

$$\dot{\rho}_{eg} = -(\frac{\gamma}{2} - \imath\delta)\rho_{eg} + \imath\frac{\Omega}{2}\rho_{gg} - \imath\frac{\Omega}{2}\rho_{ee} \tag{2.2}$$

Where $\gamma = \frac{1}{T_1}$, T_1 being the radiative atomic lifetime. $\delta = \omega_{tooth} - \omega_{eg}$ is the detuning of the closest tooth to the transition. $\Omega = \langle e| \, |\mu_{eg} \cdot E(t) \, |g\rangle$ is the Rabi frequency. The density matrix is given by

$$\rho = \begin{pmatrix} \rho_{ee} & \rho_{eg} \\ \rho_{ge} & \rho_{gg} \end{pmatrix} \tag{2.3}$$

where ρ_{ee} and ρ_{gg} are the excited and ground state populations. ρ_{eg} and ρ_{ge} are known as coherences.

The density matrix just before a pulse is $\rho^{(-)}$ and right after the pulse it is $\rho^{(+)}$ [6] [8], where

$$\rho^{(+)} = e^{i\frac{\theta}{2}\hat{\sigma}_\phi}\rho^{(-)}e^{-i\frac{\theta}{2}\hat{\sigma}_\phi} \tag{2.4}$$

and $\theta = \int dt\Omega(t)$ is the pulse area and ϕ is the carrier envelope phase

aquired by the mode-locked laser from pulse to pulse, with $\hat{\sigma}_\phi = \cos(\phi)\hat{\sigma}_x + \sin(\phi)\hat{\sigma}_y$. $\sigma_{x,y}$ are the Pauli spin matrices. The time between pulses, the density matrix evolves as

$$\rho_{ee}^{(+)}(t) = \rho_{ee}^{(+)} e^{-\gamma t} \tag{2.5}$$

$$\rho_{eg}^{(+)}(t) = \rho_{eg}^{(+)} e^{-(\frac{\gamma}{2} - i\delta)t} \tag{2.6}$$

Let us derive what the steady state ρ_{ee} population by noting that $\rho^{(-)} = \rho^{(+)}(T_r)$, where $T_r = \frac{1}{f_{\text{rep}}}$.
Let us first apply a pulse onto our two level system.

$$e^{i\frac{\theta}{2}\hat{\sigma}_\phi} = \cos(\frac{\theta}{2})\mathbb{1} + i\sin(\frac{\theta}{2})\hat{\sigma}_\phi \tag{2.7}$$

$$\hat{\sigma}_\phi = \cos(\phi)\hat{\sigma}_x + \sin(\phi)\hat{\sigma}_y \tag{2.8}$$

$$= \begin{pmatrix} 0 & e^{-i\phi} \\ e^{i\phi} & 0 \end{pmatrix} \tag{2.9}$$

$$e^{i\frac{\theta}{2}\hat{\sigma}_\phi} = \begin{pmatrix} \cos(\frac{\theta}{2}) & i\sin(\frac{\theta}{2})e^{-i\phi} \\ i\sin(\frac{\theta}{2})e^{i\phi} & \cos(\frac{\theta}{2}) \end{pmatrix} \tag{2.10}$$

Plugging equation2.10 into 2.4 we obtain

$$e^{i\frac{\theta}{2}\hat{\sigma}_\phi}\rho^{(-)}e^{-i\frac{\theta}{2}\hat{\sigma}_\phi} =$$
$$\begin{pmatrix} \cos(\frac{\theta}{2}) & i\sin(\frac{\theta}{2})e^{-i\phi} \\ i\sin(\frac{\theta}{2})e^{i\phi} & \cos(\frac{\theta}{2}) \end{pmatrix} \begin{pmatrix} \rho_{ee}^{(-)} & \rho_{eg}^{(-)} \\ \rho_{ge}^{(-)} & \rho_{gg}^{(-)} \end{pmatrix} \begin{pmatrix} \cos(\frac{\theta}{2}) & -i\sin(\frac{\theta}{2})e^{-i\phi} \\ -i\sin(\frac{\theta}{2})e^{i\phi} & \cos(\frac{\theta}{2}) \end{pmatrix} \tag{2.11}$$

Expanding this set of equations,

$$\begin{aligned} \rho_{ee}^{(+)} =& \cos^2(\frac{\theta}{2})\rho_{ee}^{(-)} + i\sin(\frac{\theta}{2})\cos(\frac{\theta}{2})e^{-i\phi}\rho_{ge}^{(-)} \\ & - i\sin(\frac{\theta}{2})\cos(\frac{\theta}{2})e^{i\phi}\rho_{eg}^{(-)} + \sin^2(\frac{\theta}{2})\rho_{gg}^{(-)} \end{aligned} \tag{2.12}$$

$$\begin{aligned} \rho_{eg}^{(+)} =& - i\sin(\frac{\theta}{2})\cos(\frac{\theta}{2})e^{-i\phi}\rho_{ee}^{(-)} + \sin^2(\frac{\theta}{2})e^{-i2\phi}\rho_{ge}^{(-)} \\ & + \cos^2(\frac{\theta}{2})\rho_{eg}^{(-)} + i\sin(\frac{\theta}{2})\cos(\frac{\theta}{2})e^{-i\phi}\rho_{gg}^{(-)} \end{aligned} \tag{2.13}$$

$$\begin{aligned} \rho_{ge}^{(+)} =& i\sin(\frac{\theta}{2})\cos(\frac{\theta}{2})e^{i\phi}\rho_{ee}^{(-)} + \sin^2(\frac{\theta}{2})e^{i2\phi}\rho_{eg}^{(-)} \\ & + \cos^2(\frac{\theta}{2})\rho_{ge}^{(-)} - i\sin(\frac{\theta}{2})\cos(\frac{\theta}{2})e^{i\phi}\rho_{gg}^{(-)} \end{aligned} \tag{2.14}$$

$$\begin{aligned} \rho_{gg}^{(+)} =& \sin^2(\frac{\theta}{2})\rho_{ee}^{(-)} - i\sin(\frac{\theta}{2})\cos(\frac{\theta}{2})e^{-i\phi}\rho_{ge}^{(-)} \\ & + i\sin(\frac{\theta}{2})\cos(\frac{\theta}{2})e^{i\phi}\rho_{eg}^{(-)} + \cos^2(\frac{\theta}{2})\rho_{gg}^{(-)} \end{aligned} \tag{2.15}$$

We can eliminate ρ_{gg} and ρ_{ge} by noting that $\rho_{ee} + \rho_{gg} = 1$ and $\rho_{ge}^* = \rho_{eg}$. This leads to

$$\rho_{ee}^{(+)} = \cos(\theta)\rho_{ee}^{(-)} + \frac{1}{2}(1-\cos(\theta)) - \frac{i}{2}\sin(\theta)(e^{i\phi}\rho_{eg}^{(-)} - e^{-i\phi}\rho_{eg}^{*(-)}) \quad (2.16)$$

$$\begin{aligned}\rho_{eg}^{(+)} =& -i\sin(\theta)e^{-i\phi}\rho_{ee}^{(-)} + \frac{i}{2}\sin(\theta)e^{-i\phi} + \frac{1}{2}e^{-i\phi}(e^{i\phi}\rho_{eg}^{(-)} + e^{-i\phi}\rho_{eg}^{*(-)}) \\ &+ \frac{1}{2}e^{-i\phi}\cos(\theta)(e^{i\phi}\rho_{eg}^{(-)} - e^{-i\phi}\rho_{eg}^{*(-)}) \end{aligned} \quad (2.17)$$

After the atom has interacted with an optical pulse, and evolved for a period of T_r, $\rho_{ee}^{(+)}(T_r) = \rho_{ee}^{(+)}e^{-\gamma T_r}$, $\rho_{eg}^{(+)}(T_r) = \rho_{eg}^{(+)}e^{-\gamma T_r/2}e^{i\delta T_r}$. Where T_r is the repitition period. [7][6][8]. Plugging this in for ρ_{ee}^{+} and $\rho_{eg}^{(+)}$ we obtain,

$$\begin{aligned}\rho_{ee}^{(+)}(T_r) =& \cos(\theta)e^{-\gamma T_r}\rho_{ee}^{(-)} + \frac{1}{2}(1-\cos(\theta))e^{-\gamma T_r} \\ &- \frac{i}{2}\sin(\theta)e^{-\gamma T_r}(e^{i\phi}\rho_{eg}^{(-)} - e^{-i\phi}\rho_{eg}^{*(-)}) \end{aligned} \quad (2.18)$$

and

$$\begin{aligned}\rho_{eg}^{(+)}(T_r) =& -i\sin(\theta)e^{-\gamma T_r/2}e^{-i(\phi-\delta T_r)}\rho_{ee}^{(-)} + \frac{i}{2}\sin(\theta)e^{-\gamma T_r}e^{-i(\phi-\delta T_r)} \\ &+ \frac{1}{2}e^{-\gamma T_r/2}e^{-i(\phi-\delta T_r)}(e^{i\phi}\rho_{eg}^{(-)} + e^{-i\phi}\rho_{eg}^{*(-)}) \\ &+ \frac{1}{2}e^{-\gamma T_r/2}e^{-i(\phi-\delta T_r)}\cos(\theta)(e^{i\phi}\rho_{eg}^{(-)} - e^{-i\phi}\rho_{eg}^{*(-)}) \end{aligned} \quad (2.19)$$

Steady state soltuion is when

$$\rho^{(-)} = \rho^{(+)}(T_r) \quad (2.20)$$

Which gives the steady state solution for ρ_{ee} and ρ_{eg} as

$$\begin{aligned}\rho_{ee} =& \cos(\theta)e^{-\gamma T_r}\rho_{ee} + \frac{1}{2}(1-\cos(\theta))e^{-\gamma T_r} \\ &- \frac{i}{2}\sin(\theta)e^{-\gamma T_r}(e^{i\phi}\rho_{eg} - e^{-i\phi}\rho_{eg}^*)\end{aligned} \tag{2.21}$$

$$\begin{aligned}\rho_{eg} =& -i\sin(\theta)e^{-\gamma T_r/2}e^{-i(\phi-\delta T_r)}\rho_{ee} + \frac{i}{2}\sin(\theta)e^{-\gamma T_r}e^{-i(\phi-\delta T_r)} \\ &+ \frac{1}{2}e^{-\gamma T_r/2}e^{-i(\phi-\delta T_r)}(e^{i\phi}\rho_{eg} + e^{-i\phi}\rho_{eg}^*) \\ &+ \frac{1}{2}e^{-\gamma T_r/2}e^{-i(\phi-\delta T_r)}\cos(\theta)(e^{i\phi}\rho_{eg} - e^{-i\phi}\rho_{eg}^*)\end{aligned} \tag{2.22}$$

This is still a coupled equation between the excited state population and coherence. We need to further decouple the two equations.

In equation 2.21, we need to eliminate ρ_{eg} and ρ_{eg}^*. Multiplying equation 2.22 by $e^{i\pm\phi}$,

$$\begin{aligned}e^{i\phi}\rho_{eg} =& -i\sin(\theta)e^{-\gamma T_r/2}e^{i\delta T_r}\rho_{ee} + \frac{i}{2}\sin(\theta)e^{-\gamma T_r/2}e^{i\delta T_r} \\ &+ \frac{1}{2}e^{i(\phi+\delta T_r)}e^{-\gamma T_r/2}(1+\cos(\theta))\rho_{eg} \\ &+ \frac{1}{2}e^{i(-\phi+\delta T_r)}e^{-\gamma T_r/2}(1-\cos(\theta))\rho_{eg}^*\end{aligned} \tag{2.23}$$

$$\begin{aligned}e^{-i\phi}\rho_{eg}^* =& i\sin(\theta)e^{-\gamma T_r/2}e^{-i\delta T_r}\rho_{ee} + \frac{-i}{2}\sin(\theta)e^{-\gamma T_r/2}e^{-i\delta T_r} \\ &+ \frac{1}{2}e^{-i(\phi+\delta T_r)}e^{-\gamma T_r/2}(1+\cos(\theta))\rho_{eg}^* \\ &+ \frac{1}{2}e^{-i(-\phi+\delta T_r)}e^{-\gamma T_r/2}(1-\cos(\theta))\rho_{eg}\end{aligned} \tag{2.24}$$

Combining equations 2.23 and 2.24

$$
\begin{aligned}
e^{i\phi}\rho_{eg} - e^{-i\phi}\rho^*_{eg} = \\
&\frac{1}{2}e^{-\gamma T_r/2}\big[\rho_{eg}(e^{i(\phi+\delta T_r)} + \cos(\theta)e^{i(\phi+\delta T_r)} - e^{i(\phi-\delta T_r)} + \cos(\theta)e^{i(\phi-\delta T_r)}) \\
&- \rho^*_{eg}(e^{-i(\phi+\delta T_r)} + \cos(\theta)e^{-i(\phi+\delta T_r)} - e^{-i(\phi-\delta T_r)} + \cos(\theta)e^{-i(\phi-\delta T_r)})\big] \\
&+ \frac{i}{2}\sin(\theta)e^{-\gamma T_r/2}(2\cos(\delta T_r))(1-2\rho_{ee}) \qquad (2.25)
\end{aligned}
$$

$$
\begin{aligned}
=&\frac{1}{2}e^{-\gamma T_r/2}\big[e^{i\phi}\rho_{eg}(2i\sin(\delta T_r) + 2\cos(\theta)\cos(\delta T_r)) \\
&- e^{-i\phi}\rho^*_{eg}(-2i\sin(\delta T_r) + 2\cos(\theta)\cos(\delta T_r))\big] \\
&+ \frac{i}{2}\sin(\theta)e^{-\gamma T_r/2}(2\cos(\delta T_r))(1-2\rho_{ee}) \qquad (2.26)
\end{aligned}
$$

Further simplifying to

$$
\begin{aligned}
e^{i\phi}\rho_{eg} - e^{-i\phi}\rho^*_{eg} \\
&= e^{-\gamma T_r/2}\big[i\sin(\delta T_r)(e^{i\phi}\rho_{eg} + e^{-i\phi}\rho^*_{eg}) + \cos(\theta)\cos(\delta T_r)(e^{i\phi}\rho_{eg} - e^{-i\phi}\rho^*_{eg})\big] \\
&+ \frac{i}{2}\sin(\theta)e^{-\gamma T_r/2}(2\cos(\delta T_r))(1-2\rho_{ee}) \qquad (2.27)
\end{aligned}
$$

Now, we need to solve for $e^{i\phi}\rho_{eg} + e^{-i\phi}\rho^*_{eg}$ and plug it back into equation 2.27

$$
\begin{aligned}
e^{i\phi}\rho_{eg} + e^{-i\phi}\rho^*_{eg} = \\
&e^{-\gamma T_r/2}\big[i\sin(\delta T_r)\cos(\theta)(e^{i\phi}\rho_{eg} - e^{-i\phi}\rho^*_{eg}) + \cos(\delta T_r)(e^{i\phi}\rho_{eg} + e^{-i\phi}\rho^*_{eg})\big] \\
&+ \frac{i}{2}\sin(\theta)e^{-\gamma T_r/2}(2\cos(\delta T_r))(1-2\rho_{ee}) \qquad (2.28)
\end{aligned}
$$

Isolating $e^{i\phi}\rho_{eg} + e^{-i\phi}\rho^*_{eg}$,

$$\left[e^{i\phi}\rho_{eg} + e^{-i\phi}\rho_{eg}^*\right]\left[1 - \cos(\delta T_r)e^{-\gamma T_r/2}\right] = \\ e^{-\gamma T_r/2}\left[i\sin(\delta T_r)\cos(\theta)(e^{i\phi}\rho_{eg} - e^{-i\phi}\rho_{eg}^*)\right] \\ - \sin(\theta)\sin(\delta T_r)e^{-\gamma T_r/2}(1 - 2\rho_{ee}) \tag{2.29}$$

$$e^{i\phi}\rho_{eg} + e^{-i\phi}\rho_{eg}^* = \frac{1}{\alpha}\Big[e^{-\gamma T_r/2}\left[i\sin(\delta T_r)\cos(\theta)(e^{i\phi}\rho_{eg} - e^{-i\phi}\rho_{eg}^*)\right] \\ - \sin(\theta)\sin(\delta T_r)e^{-\gamma T_r/2}(1 - 2\rho_{ee})\Big] \tag{2.30}$$

Where $\alpha = 1 - \cos(\delta T_r)e^{-\gamma T_r/2}$. Plugging equation 2.30 into 2.27, we obtain

$$e^{i\phi}\rho_{eg} - e^{-i\phi}\rho_{eg}^* = \\ e^{-\gamma T_r/2}\Bigg\{\frac{i\sin(\delta T_r)}{\alpha}\left[e^{-\gamma T_r/2}\left(i\sin(\delta T_r)\cos(\theta)(e^{i\phi}\rho_{eg} - e^{-i\phi}\rho_{eg}^*)\right)\right. \\ \left. - \sin(\theta)\sin(\delta T_r)e^{-\gamma T_r/2}(1 - 2\rho_{ee})\right] + \cos(\theta)\cos(\delta T_r)(e^{i\phi}\rho_{eg} - e^{-i\phi}\rho_{eg}^*)\Bigg\} \\ + i\sin(\theta)\cos(\delta T_r)e^{-\gamma T_r/2}(1 - 2\rho_{ee}) \tag{2.31}$$

Further simplifying the equation to be

$$\left[e^{i\phi}\rho_{eg} - e^{-i\phi}\rho_{eg}^*\right]\left[1 + \frac{e^{-\gamma T_r}}{\alpha}\sin^2(\delta T_r)\cos(\theta) - e^{-\gamma T_r/2}\cos(\theta)\cos(\delta T_r)\right] = \\ - \frac{i\sin^2(\delta T_r)}{\alpha}\sin(\theta)e^{-\gamma T_r}(1 - 2\rho_{ee}) + i\sin(\theta)\cos(\delta T_r)e^{-\gamma T_r/2}(1 - 2\rho_{ee}) \tag{2.32}$$

Finally we have an equation where $e^{i\phi}\rho_{eg} - e^{-i\phi}\rho_{eg}^*$ is independent of ρ_{eg} or

ρ_{eg}^*

$$e^{i\phi}\rho_{eg} - e^{-i\phi}\rho_{eg}^* = \frac{1}{\beta}\big[(1-2\rho_{ee})(i\sin(\theta)e^{-\gamma T_r/2})\big(- \frac{1}{\alpha}\sin^2(\delta T_r)e^{-\gamma T_r/2} + \cos(\delta T_r)\big)\big] \tag{2.33}$$

Let us simplify $\beta = 1 + \frac{e^{-\gamma T_r}}{\alpha}\sin^2(\delta T_r)\cos(\theta) - e^{-\gamma T_r/2}\cos(\theta)\cos(\delta T_r)$

$$\beta = 1 + \left[\frac{e^{-\gamma T_r}\sin^2(\delta T_r) - e^{-\gamma T_r/2}\cos(\delta T_r) + \cos^2(\delta T_r)e^{-\gamma T_r}}{1-\cos(\delta T_r)e^{-\gamma T_r/2}}\right]\cos(\theta)$$

$$= \frac{1-\cos(\delta T_r)e^{-\gamma T_r/2} + e^{-\gamma T_r}\cos(\theta) - e^{-\gamma T_r/2}\cos(\delta T_r)\cos(\theta)}{1-\cos(\delta T_r)e^{-\gamma T_r/2}}$$

$$= \frac{1 + e^{-\gamma T_r}\cos(\theta) - \cos(\delta T_r)e^{-\gamma T_r/2}(1+\cos(\theta))}{1-\cos(\delta T_r)e^{-\gamma T_r/2}} \tag{2.34}$$

Going back to equation 2.33,

$$e^{i\phi}\rho_{eg} - e^{-i\phi}\rho_{eg}^* =$$
$$\frac{1}{\beta}\left[(1-2\rho_{ee})(i\sin(\theta)e^{-\gamma T_r/2})\left(\frac{-sin^2(\delta T_r)e^{-\gamma T_r/2} + \cos^2(\delta T_r)e^{-\gamma T_r/2}}{1-\cos(\delta T_r)e^{-\gamma T_r/2}}\right)\right]$$
$$= (1-2\rho_{ee})(i\sin(\theta)e^{-\gamma T_r/2})\left[\frac{\cos(\delta T_r) - e^{-\gamma T_r/2}}{(1+e^{-\gamma T_r}\cos(\theta)) - \cos(\delta T_r)e^{-\gamma T_r/2}(1+\cos(\theta))}\right]$$
$$= (1-2\rho_{ee})(i\sin(\theta))\left[\frac{\cos(\delta T_r) - e^{-\gamma T_r/2}}{(e^{\gamma T_r/2} + e^{-\gamma T_r/2}\cos(\theta)) - \cos(\delta T_r)(1+\cos(\theta))}\right] \tag{2.35}$$

With $e^{i\phi}\rho_{eg} - e^{-i\phi}\rho_{eg}^*$ now only depending on ρ_{ee}, we can plug equation 2.35 back into equation 2.21

$$\rho_{ee}(1-\cos(\theta)e^{-\gamma T_r}) = \frac{1}{2}(1-\cos(\theta)e^{-\gamma T_r})$$
$$-\frac{i}{2}\sin(\theta)e^{-\gamma T_r}\big[(1-2\rho_{ee})(i\sin(\theta))\big]\left[\frac{\cos(\delta T_r)-e^{-\gamma T_r/2}}{(e^{\gamma T_r/2}+e^{-\gamma T_r/2}\cos(\theta))-\cos(\delta T_r)(1+\cos(\theta))}\right] \tag{2.36}$$

Isolating ρ_{ee},

$$\rho_{ee}\left[1-\cos(\theta)e^{-\gamma T_r}+\sin^2(\theta)e^{-\gamma T_r}\left[\frac{\cos(\delta T_r)-e^{-\gamma T_r/2}}{(e^{\gamma T_r/2}+e^{-\gamma T_r/2}\cos(\theta))-\cos(\delta T_r)(1+\cos(\theta))}\right]\right] =$$
$$\frac{1}{2}(1-\cos(\theta))e^{-\gamma T_r}+\frac{1}{2}\sin^2(\theta)e^{-\gamma T_r}\left[\frac{\cos(\delta T_r)-e^{-\gamma T_r/2}}{(e^{\gamma T_r/2}+e^{-\gamma T_r/2}\cos(\theta))-\cos(\delta T_r)(1+\cos(\theta))}\right] \tag{2.37}$$

Simplifying the term on LHS

$$A \equiv 1-\cos(\theta)e^{-\gamma T_r}+\sin^2(\theta)e^{-\gamma T_r}\left[\frac{\cos(\delta T_r)-e^{-\gamma T_r/2}}{(e^{\gamma T_r/2}+e^{-\gamma T_r/2}\cos(\theta))-\cos(\delta T_r)(1+\cos(\theta))}\right]$$
$$= \frac{e^{\gamma T_r/2}-\cos(\delta T_r)(1+\cos(\theta))(1-e^{-\gamma T_r})-e^{-3\gamma T_r/2}}{(e^{\gamma T_r/2}+-\gamma T_r/2)\cos(\theta)-\cos(\delta T_r)(1+\cos(\theta))} \tag{2.38}$$

Going back to equation 2.37, we get

$$\rho_{ee} =$$
$$\frac{1}{A}\left[\frac{1}{2}(1-\cos(\theta))e^{-\gamma T_r}+\frac{1}{2}\sin^2(\theta)e^{-\gamma T_r}\left[\frac{\cos(\delta T_r)-e^{-\gamma T_r/2}}{(e^{\gamma T_r/2}+e^{-\gamma T_r/2}\cos(\theta))-\cos(\delta T_r)(1+\cos(\theta))}\right]\right] \tag{2.39}$$

$$\rho_{ee} =$$
$$\frac{e^{-\gamma T_r}}{2}\left[\frac{e^{\gamma T_r/2} - \cos(\theta)(e^{\gamma T_r/2} - e^{-\gamma T_r/2}) - \cos(\delta T_r) - e^{-\gamma T_r/2} + \cos(\delta T_r)}{e^{\gamma T_r/2} - \cos(\delta T_r)(1+\cos(\theta))(1-e^{-\gamma T_r}) - e^{-3\gamma T_r/2}}\right]$$
$$= \frac{e^{-\gamma T_r}}{2}\left[\frac{4\sin^2(\frac{\theta}{2})\sinh(\frac{\gamma T_r}{2})}{e^{\gamma T_r/2}(1-e^{-2\gamma T_r}) - \cos(\delta T_r)(1+\cos(\theta))(1-e^{-\gamma T_r})}\right] \quad (2.40)$$

The steady state scattering rate is given by [6]

$$\Gamma_{ss} = \frac{1}{T_r}(\rho_{ee} - \rho_{ee}(T_r)) \quad (2.41)$$
$$\frac{1}{T_r}\rho_{ee}(1 - e^{-\gamma T_r}) \quad (2.42)$$

Using equation 2.40 and 2.41, we get

$$\Gamma_{ss}(\delta) = \frac{e^{-\gamma T_r}}{2}\left[\frac{4\sin^2(\frac{\theta}{2})\sinh(\frac{\gamma T_r}{2})}{e^{\gamma T_r/2}(1-e^{-2\gamma T_r}) - \cos(\delta T_r)(1+\cos(\theta))(1-e^{-\gamma T_r})}\right](e^{\gamma T_r} - 1)$$
$$\Gamma_{ss}(\delta) = \frac{\sin^2(\frac{\theta}{2})\sinh(\frac{\gamma T_r}{2})}{\cosh(\frac{\gamma T_r}{2}) - \cos(\delta T_r)\cos^2(\frac{\theta}{2})} \quad (2.43)$$

2.2 Cycle average amplification and damping

If we include micromotion into account, the scattering rate from a CW laser is [27]

$$\gamma(\delta, v(t)) = \frac{\gamma}{2}\frac{I}{I_{sat}}\sum_{n=-\infty}^{\infty}\frac{J_n^2\left[\sqrt{2}\frac{kv_0}{\Omega_{\rm rf}}\cos(\omega_{sec}t)\right]}{1 + s_0 + \frac{4}{\gamma^2}(\delta + n\Omega_{\rm rf} + kv_0\sin(\omega_{sec}t))^2} \quad (2.44)$$

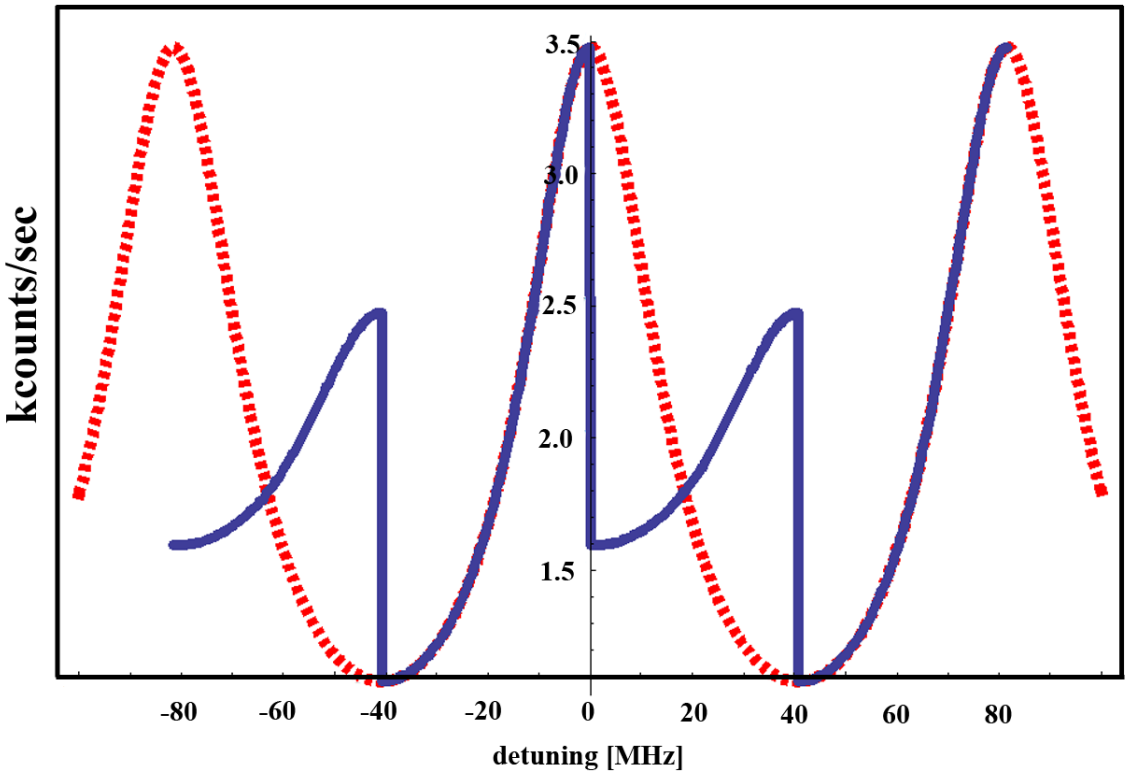

Figure 2.1: Theoretical fluorescence spectrum of a trapped ion illuminated by an optical frequency comb. When the nearest comb tooth is red-detuned, the ion is follows the rest-frame line shape (dashed red curve). When the nearest comb tooth is blue detuned, the fluorescence does not decay as a lorentzian, but has a rising slope instead. When the nearest tooth is blue detuned, we will see that the ion is outstretched into into one of its cooling secular motion.

where J_n is the n^{th} order Bessel function of the 1st kind, I and I_{sat} are the intensity and saturation intensity, $s_0 = \frac{I}{I_{sat}}$, $\delta = \omega_{laser} - \omega_{atom}$

We can calculate the cylce average scattering rate over a period of secular motion,

$$\Gamma_{cw}(\delta, v(t)) = \frac{1}{2\pi}\int_0^{2\pi} d\xi \frac{\gamma}{2}\frac{I}{I_{sat}} \sum_{n=-\infty}^{\infty} \frac{J_n^2\left[\sqrt{2}\frac{kv_0}{\Omega_{\mathrm{rf}}}\cos(\xi)\right]}{1 + s_0 + \frac{4}{\gamma^2}(\delta + n\Omega_{\mathrm{rf}} + kv_0\sin(\xi))^2} \tag{2.45}$$

where $\xi = \omega_{sec}t$

Combining our results from the previous section for the scattering rate of an ion at rest due to an optical frequency comb and including micromotion,

$$\Gamma_{fc} = I\sum_{n=-\infty}^{\infty} \frac{J_n^2\left[\sqrt{2}\frac{\vec{k}\cdot\vec{v}}{\Omega_{\mathrm{rf}}}\cos(\omega_{sec}t)\right]\sin^2(\frac{\theta}{2})\sinh(\frac{\gamma T_r}{2})}{\cosh(\frac{\gamma T_r}{2}) - \cos(\delta T_r)\cos^2(\frac{\theta}{2})} \tag{2.46}$$

The secular-cycle-averaged scattering rate is given by

$$\Gamma_{\mathrm{avg}}(\delta, x_0) = \frac{1}{2\pi}\int_0^{2\pi} d\xi \sum_{n=-\infty}^{\infty} J_n^2\left[\sqrt{2}\frac{kv_0}{\Omega_{\mathrm{rf}}}\cos(\xi)\right] \times \Gamma_{ss}(\delta + n\Omega_{\mathrm{rf}} + k\omega_x x_0\sin(\xi)) \tag{2.47}$$

Figure 2.1 is a plot of equation 2.47. The steady state scattering rate of an ion illuminated by an optical frequency comb has different features depending on if the closest comb tooth is red detuned or blue detuned. If the closest tooth to resonance is red detuned, it follows would would be the rest-frame scattering rate as shown by the dashed red curve. If the closest tooth is blue detuned, the fluorescence will not decay as if it were illuminated by a CW laser, but instead have this steady state of increase until the closest tooth is once again red detuned.

The rate of energy transfer from the optical frequency comb to the ion's motion is given by [9]

$$\frac{dE}{dt} = -\beta(E)\frac{2E}{m} + S(E). \tag{2.48}$$

$S(E) = (1+\zeta)\frac{\hbar^2|k|^2}{2m}\Gamma_{fc}(\delta, x_0)$ is the stochastic heating power due to spontaneous emission, with $\zeta = \frac{2}{5}$ being the geometric factor for dipole emission and $E = \frac{1}{2}m\omega_{sec}^2 x_0^2$ is the secular energy of the ion. The coherent amplification power is given by $-\beta 2E/m = \langle \vec{F} \cdot \vec{v}_{sec}(\xi)\rangle_\xi$, which gives

$$\beta(E) = \frac{\hbar k}{2\pi\omega x_0}\int_0^{2\pi} d\xi \sin(\xi)\Gamma_{fc}(\delta + n\Omega_{\text{rf}} + k\omega x_0 \sin(\xi)) \tag{2.49}$$

Equation 2.48 can be understood as having a heating term and a cooling term. $S(E)$ is always a heating term, and depending on the sign of $\beta(E)$, the 1st term can either damp the motion or amplify the oscillation. Looking at 2.2, when the nearest resonant comb tooth is on the blue detuned, $\beta < 0$. This amplification has recently been observed spectroscopically as a line pulling mechanism[16]. The frequency comb will add energy to the motion of an initially cold ion until the net power transfer vanishes, leading to steady-state oscillation. Multiple roots exist for equation 2.48 for a given detuning. These roots the stable fixed points represented by green dots in 2.2.

2.3 Fast Pulse regime

The previous section dealt with the interaction of an ion with an optical frequency comb where the pulse to pulse seperation is is on the order of 10's of ns. We have also ran experiments in the regime where the pulse to pulse seperation is on the orders of 100's of ps. This can be achieved

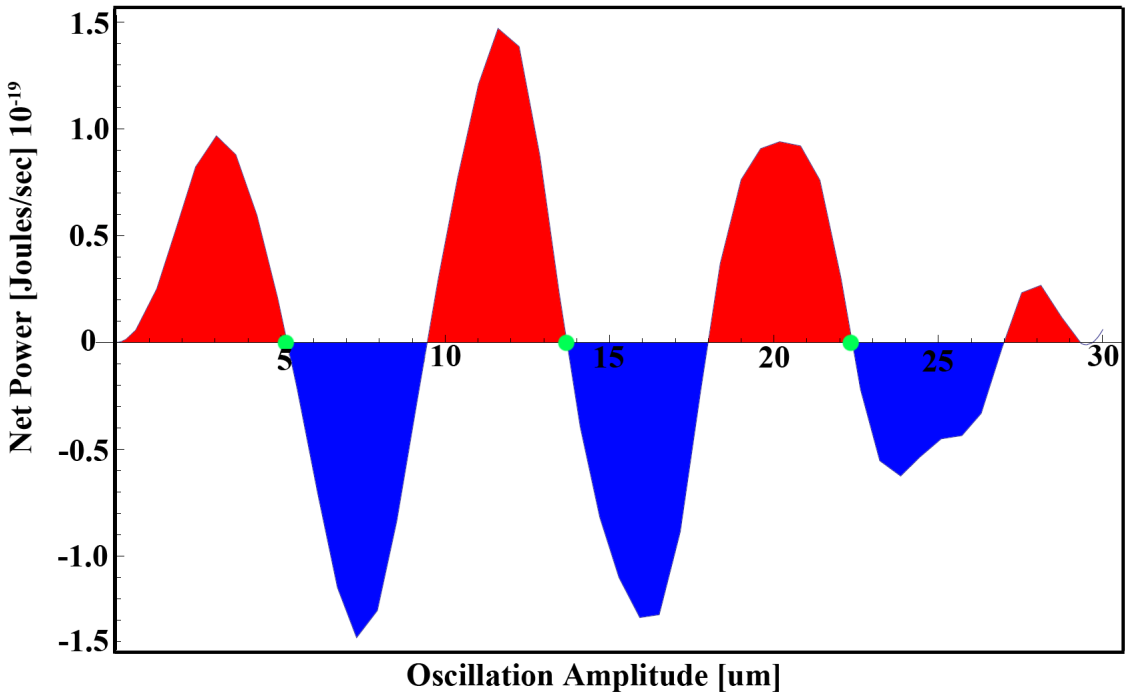

Figure 2.2: Calculated net power delivered to motion of trapped ion illuminated by an optical frequency comb as a function of oscillation amplitude in the trap. Equation 2.48 is plotted for $\delta = \pi/2T_r$. Red (blue) shading indicates amplification (damping) of the ion's motion. Green dots represent stable fixed points

with a Mach-Zender interferometer, where a single pulse is split into 2 by a beam splitter and recombined later with one leg of the interferometer being slightly longer than the other [28].

Let us first take a look at how much optical power is required to generate a π pulse for an S to P transition.

$$\Omega_{rabi}(t) = \gamma\sqrt{\frac{I(t)}{2I_{sat}}} \tag{2.50}$$

Where $\gamma = 1/\tau$, τ is the radiative lifetime, $I_{sat} = \frac{\pi hc}{3\lambda^3\tau}$ is the saturation

intensity and $I(t)$ is the optical intensity. For a mode-locked laser pulses, the electric field envelope is theoretically given by a hyperbolic secant [10]. Hence, the intensity goes as

$$I(t) = I_0 \text{sech}^2(\frac{\pi t}{T_p}) \tag{2.51}$$

Where I_0 is the peak intensity of the pulse. It is typically easier to work with time averaged intensity, since we typically measure the time averaged power of the laser instead of the peak power. The average intensity is given by

$$\bar{I} = \frac{1}{T_r}\int_{-\infty}^{\infty} dt I_0 \text{sech}^2(\frac{\pi t}{T_p}) = \frac{2T_p}{\pi T_r} \tag{2.52}$$

Relating this to the average power,

$$\begin{aligned} \bar{I} &= \frac{\bar{P}}{A} \\ I_0 &= \frac{\pi \bar{P} T_r}{2AT_p} \end{aligned} \tag{2.53}$$

where $A = \pi\omega_0^2$ (ω_0 being the $1/e^2$ intensity of the beam).
The integrated Rabi frequency is the pulse area,

$$\int_{-\infty}^{\infty} \Omega_{rabi}(t)dt = \int_{-\infty}^{\infty} \gamma\sqrt{\frac{I_0}{2I_{sat}}} sech(\frac{\pi t}{T_p})dt = \pi$$

$$\pi = \sqrt{\frac{\pi T_r \bar{P}}{4AT_p I_{\text{sat}}}} T_p \gamma \tag{2.54}$$

Solving for the average power, we obtain

$$\bar{P}_\pi = \frac{4\pi I_{\text{sat}}}{\gamma^2 T_r T_p} \tag{2.55}$$

Where $A = \pi\omega_0^2$ (ω_0 being the $1/e^2$ intensity of the beam), and Γ is the gamma function. Our experimental setup, with $\omega_0 \approx 25\mu m$, $T_p \approx 10ps$, $T_r = 12.5ns$, $\lambda = 369.5nm$, we would need about 3.6 mW to achieve a π pulse.

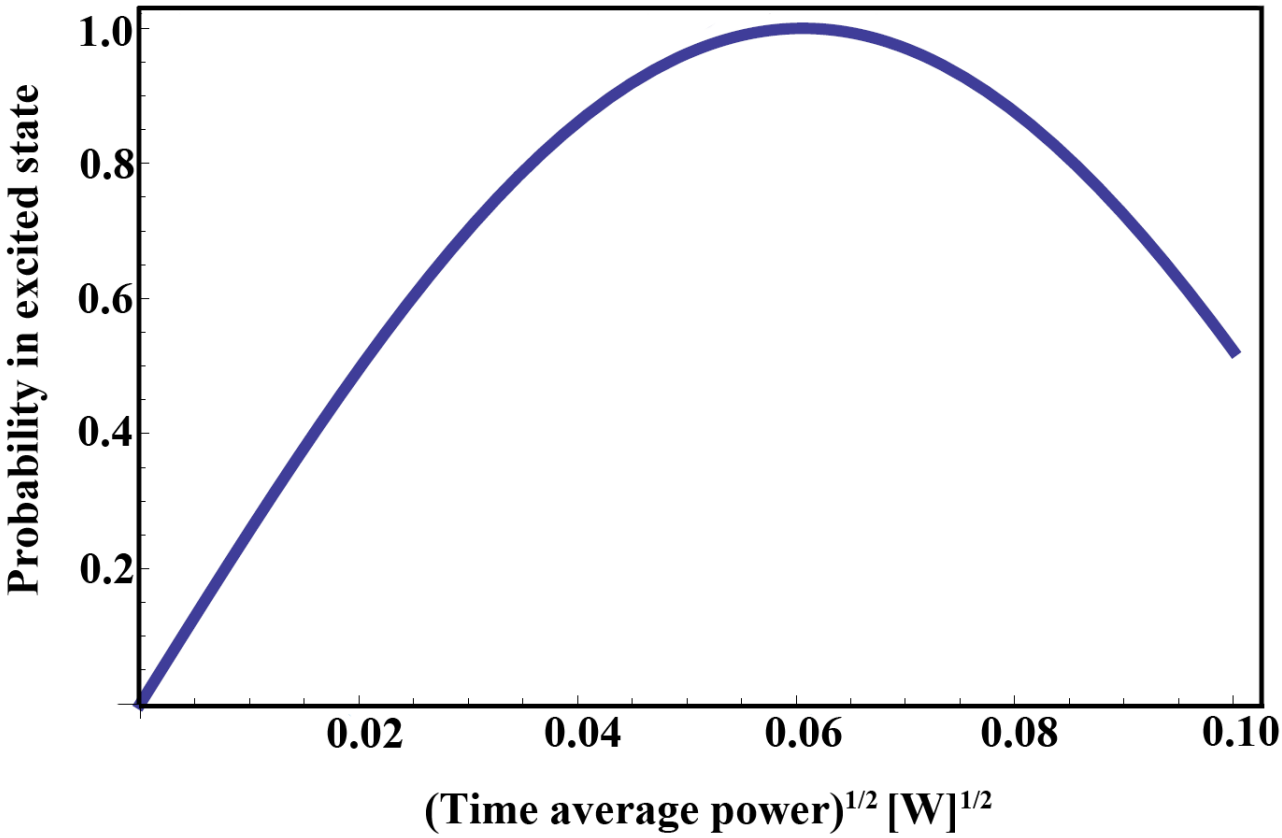

Figure 2.3: Plot of (time average power)$^{1/2}$ vs population in the excited state. Parameters are $T_p = 10$ ps, $\omega_0 = 25$ μm, $T_r = 12.5$ ns, $\lambda = 369.5$ nm. $\pi-$ pulse condition is when $\bar{P} = 3.6$ mW

CHAPTER 3

Ultrafast state detection

Projective readout of quantum information stored in atomic qubits typically uses state-dependent CW laser-induced fluorescence [29]. This method requires an often sofisticated imaging system to spatially filter out background CW laser light. An alternative approach to spatially filtering the signal, is to temporally filter the light collected through pulse sequences that are timed accordingly. Before we dive into how this scheme works, let us review how state readout works traditionally with ions.

3.1 Ytterbium Qubit

Much effort has been put in to try to maniupulate a handful of qubits together. One of the main reasons to be able to control and manipulate qubits is to perform quantum computation with qubits. A quantum bit (qubit) is simply an arbtitrary superposition of 2 quantum states.

$$|\psi\rangle = \alpha\,|0\rangle + \beta\,|1\rangle \tag{3.1}$$

where α and β are arbitrary complex numbers that satisfy $|\alpha|^2 + |\beta|^2 = 1$. The power of quantum computation can be found in these references [18] [29][30][34][33].

There are a number of choices that can be made in choosing an trapped ion qubit [32] [31] [19]. The following requirements must be met in order to

perform quantum computations: qubit state initilization, qubit operation and state readout. The fidelity (how much you trust what you think you did) of each of these three steps is crucial to determine how reliable and reproducable each experiment is.

In order to initialize the state of a qubit, we first need to Doppler cool the ions. Second, the ion needs to be optically pumped into either the dark state or bright state. From a technological standpoint, we would like to have as much laser cooling power as possible, which makes Ytterbium a decent choice, as 369 nm light is not terribly hard to produce. The nuclear 1/2 spin makes the qubit magnetically insensitive to 1st order. It also allows simple and efficient state preperation and detection. Denoting the ${}^2S_{1/2}\left|F=1,m_f=0\right\rangle$ as the bright state and ${}^2S_{1/2}\left|F=0,m_f=0\right\rangle$ as the dark state, our qubit is seperated by 12.6 GHz.

In the previous section, we discussed how Doppler cooling works with ${}^{174}\mathrm{Yb}^+$, 3.3 is the ${}^{171}\mathrm{Yb}^+$ energy diagram for Doppler cooling. The extra complexity lies in the non zero nuclear spin, which gives rise to hyperfine splittings. In order to Doppler cool, we simply add sidebands on the main 369 nm light at 14.7 GHz, which connects all possible states. This is done by sending the light through an electro-optical modulator (EOM).

The next step is to optically pump the ion into the dark state. This is typically done by turning the Doppler cooling light off and turning the optical pump beam on, which is the same frequency as the Doppler cooling beam without the sidebands. Once the ion is pumped dark, qubit manipulations can be done followed by state readout. State readout is performed by shining light which is resonant with ${}^2P_{1/2}\left|F=0,m_f=0\right\rangle$ and ${}^2S_{1/2}\left|F=1,m_f=0\right\rangle$. If the qubit is in state $|1\rangle$, then the ion will fluoresce. If the ion was in the $|0\rangle$ state, then the ion will not fluoresce, since the state is 12.6 GHz blue detuned from the laser.

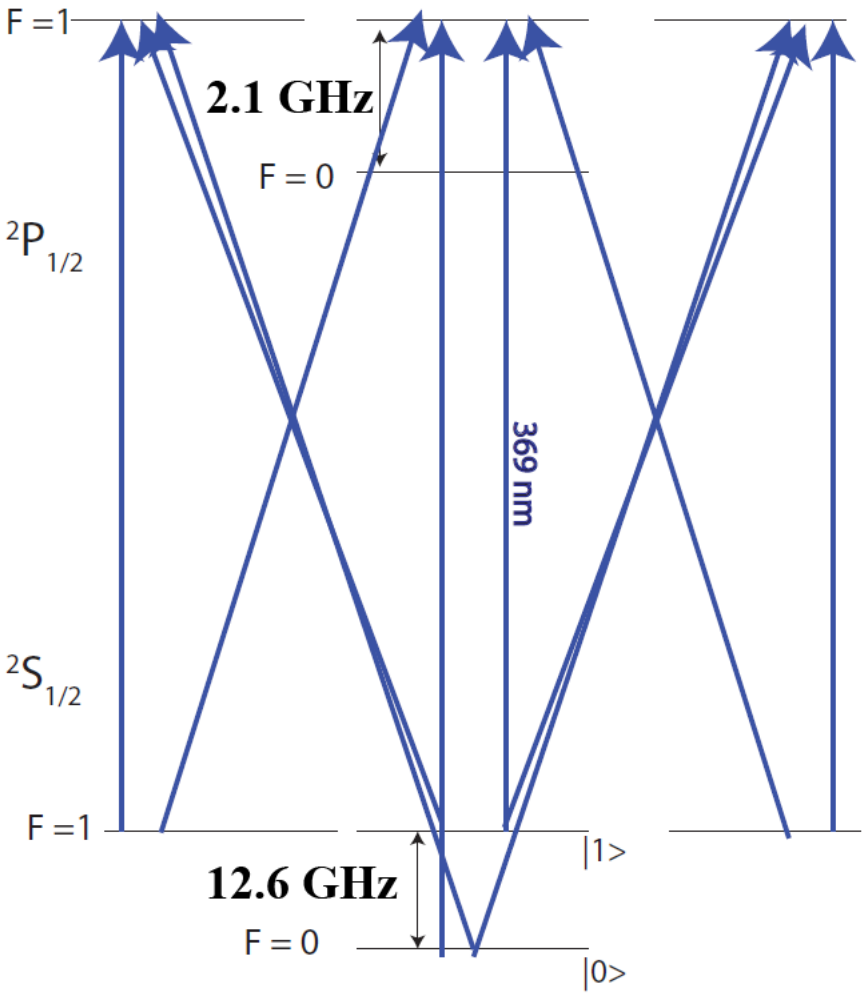

Figure 3.1: The non zero hyperfine splitting requires additional sidebands to Doppler cool $^{171}Yb^{+}$. We use the second order sideband from an EOM at 14.7 GHz to connect $^{2}S_{1/2}\,|F=0\rangle$ to $^{2}P_{1/2}\,|F=1\rangle$ manifold.

An alternative approach to state detection is by temporally seperating our background scatter and ion fluorescence signal. The idea is that we use a sequence of optical pulses to carve out a spectrum which only has light on the transition which we want to drive ($^{2}S_{1/2}\,|F=0,m_F=0\rangle \rightarrow {}^{2}P_{1/2}\,|F=0,m_F=0\rangle$), and minimal to no light in all of the other possible transitions. The pair of pulses interact with the ion on the 100s ps

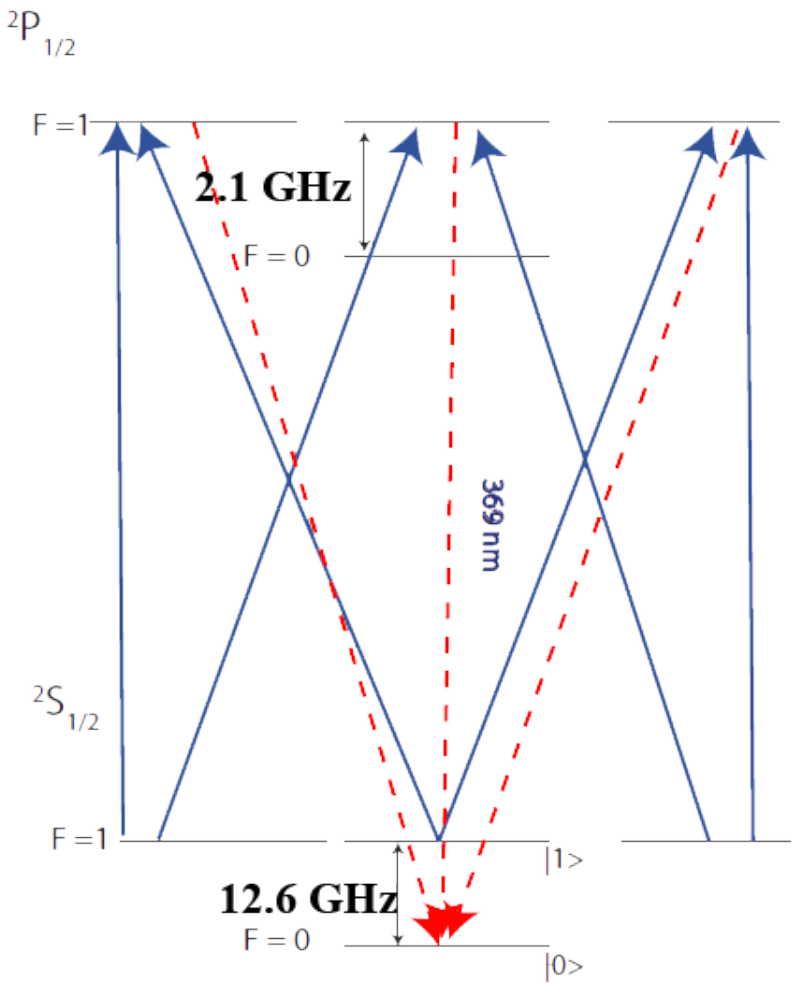

Figure 3.2: State initialization is typically performed by shining 369.5 nm light on resonant with $^2S_{1/2}\,|F=1\rangle$ to $^2P_{1/2}\,|F=1\rangle$ manifold. The ion can either fall back down to the $|F=1\rangle$ manifold or drop to the $^2S_{1/2}\,|F=0\rangle$ state. Since the laser light is 12.6 GHz detuned from transition, the ion will be optically pumped into the $^2S_{1/2}\,|F=0\rangle$ state.

time scale, while the decay time of the ion happens on the 10s ns time scale. If there is a click on the PMT in the time when we know there is no mode-locked laser light, then the signal must be from the ion.

There are a total of 8 states that come into play between $^2S_{1/2}$ and $^2P_{1/2}$ manifolds. Our goal is to time the pair of pulses properly such that we only drive the desired transition of $^2S_{1/2}\,|F=1\rangle$ to $^2P_{1/2}\,|F=0\rangle$ while

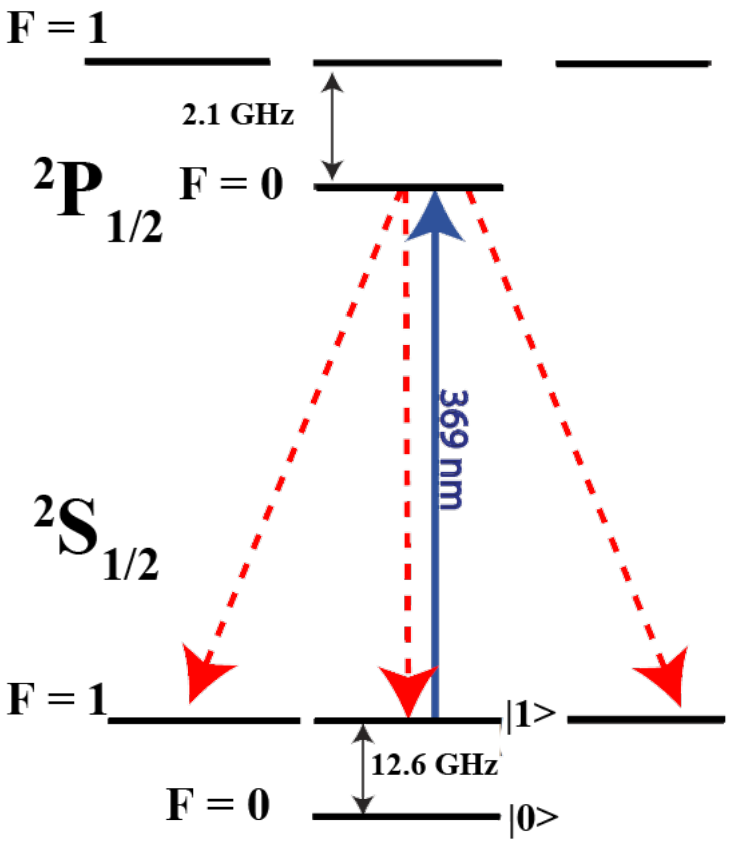

Figure 3.3: State detection is performed by shining 369.5 nm light resonant between $^2\mathrm{S}_{1/2}\,|F=1\rangle$ to $^2\mathrm{P}_{1/2}\,|F=0\rangle$ states. If the ion is in the $|1\rangle$ state, it will fluoresce, while staying dark if it were in the $|0\rangle$ state.

suppressing all other transitions. In theory, we could use an infinite number of optical pulses to carve a frequency spectrum that perfectly matches the desired transition while suppressing all other transtions. But due to technical dificulties of stabilizing many delay stages, let us first calculate the final state probability after only a pair of optical pulses.

The Hamiltonian of an ion with 8 levels interacting with a square pulse of light is given by

$$\hat{H} = \frac{\tau}{2}\begin{pmatrix} 0 & 0 & 0 & 0 & 0 & \Omega_{05} & \Omega_{06} & \Omega_{07} \\ 0 & 0 & 0 & 0 & \Omega_{14} & \Omega_{15} & \Omega_{16} & \Omega_{17} \\ 0 & 0 & 0 & 0 & \Omega_{24} & \Omega_{25} & \Omega_{26} & 0 \\ 0 & 0 & 0 & 0 & \Omega_{34} & 0 & \Omega_{36} & \Omega_{37} \\ 0 & \Omega_{14} & \Omega_{24} & \Omega_{34} & 0 & 0 & 0 & 0 \\ \Omega_{05} & \Omega_{15} & \Omega_{25} & 0 & 0 & 0 & 0 & 0 \\ \Omega_{06} & \Omega_{16} & \Omega_{26} & \Omega_{36} & 0 & 0 & 0 & 0 \\ \Omega_{07} & \Omega_{17} & \Omega_{27} & \Omega_{37} & 0 & 0 & 0 & 0 \end{pmatrix} \tag{3.2}$$

Where τ is the pulse duration and Ω_{nm} is the Rabi frequency. The Rabi frequency can be calculated using the Wigner-Eckart theorem

$$\Omega_{\mathrm{nm}} = C(F_{\mathrm{n}}, m_{F_{\mathrm{n}}}, J_{\mathrm{n}}, F_{\mathrm{m}}, m_{F_{\mathrm{m}}}, J_{\mathrm{m}}, I, q)\gamma\sqrt{\frac{I}{2I_{\mathrm{sat}}}} \tag{3.3}$$

where

$$C(F_{\mathrm{n}}, m_{F_{\mathrm{n}}}, J_{\mathrm{n}}, F_{\mathrm{m}}, m_{F_{\mathrm{m}}}, J_{\mathrm{m}}, I, q) =$$
$$(-1)^{J_{\mathrm{m}}+I-m_{F_{\mathrm{m}}}}\sqrt{(2F_{\mathrm{n}}+1)(2F_{\mathrm{m}}+1)}\begin{Bmatrix} J_{\mathrm{m}} & F_{\mathrm{m}} & I \\ F_{\mathrm{n}} & J_{\mathrm{n}} & 1 \end{Bmatrix}\begin{pmatrix} F_{\mathrm{n}} & 1 & F_{\mathrm{m}} \\ m_{F_{\mathrm{n}}} & q & -m_{F_{\mathrm{m}}} \end{pmatrix} \tag{3.4}$$

The coefficient $C(F_{\mathrm{n}}, m_{F_{\mathrm{n}}}, J_{\mathrm{n}}, F_{\mathrm{m}}, m_{F_{\mathrm{m}}}, J_{\mathrm{m}}, I, q)$ gives the relative transition strength between different states. J represents the total electron angular momentum $L+S$. F represents the total atomic angular momentum $I+J$, where I is the nuclear spin. m_F is the angular momentum projection. q indicates the polarization, with $q=-1$ is σ^- polarized, $q=0$ is π polarized,

and $q = +1$ is σ^+ polarized. The reduced matrix element are Wigner 6j and 3j symbols. For $^{171}\mathrm{Yb}^+$, $S = 1/2$ and $I = 1/2$.

We would like to solve for the probabilty of being in each of the 8 states after a 2 pulse sequence. The evolution operator is given by

$$\hat{U} = e^{-i\hat{H}} \tag{3.5}$$

Assuming the ion initially started in the bright state $^2\mathrm{S}_{1/2}\,|F = 1, m_F = 1\rangle$. After the first pulse hits the ion. The states evolve as

$$\begin{bmatrix} \psi_0 \\ \psi_1 \\ \psi_2 \\ \psi_3 \\ \psi_4 \\ \psi_5 \\ \psi_6 \\ \psi_7 \end{bmatrix} = \hat{U} \begin{bmatrix} 0 \\ 1 \\ 0 \\ 0 \\ 0 \\ 0 \\ 0 \\ 0 \end{bmatrix} \tag{3.6}$$

The ion then freely evolves for a time t_d before the next pulse arrives. The free evolution of the states are given by

$$\begin{bmatrix} \psi_0(t_\mathrm{d}) \\ \psi_1(t_\mathrm{d}) \\ \psi_2(t_\mathrm{d}) \\ \psi_3(t_\mathrm{d}) \\ \psi_4(t_\mathrm{d}) \\ \psi_5(t_\mathrm{d}) \\ \psi_6(t_\mathrm{d}) \end{bmatrix} = \begin{bmatrix} \psi_0 e^{-i\omega_0 t_d} \\ \psi_1 e^{-i\omega_1 t_d} \\ \psi_2 e^{-i\omega_2 t_d} \\ \psi_3 e^{-i\omega_3 t_d} \\ \psi_4 e^{-i\omega_4 t_d} \\ \psi_5 e^{-i\omega_5 t_d} \\ \psi_6 e^{-i\omega_6 t_d} \\ \psi_7 e^{-i\omega_7 t_d} \end{bmatrix} \tag{3.7}$$

The second pulse arrives and the final wave function is given by

$$\begin{bmatrix} \psi_{0_\mathrm{final}} \\ \psi_{1_\mathrm{final}} \\ \psi_{2_\mathrm{final}} \\ \psi_{3_\mathrm{final}} \\ \psi_{4_\mathrm{final}} \\ \psi_{5_\mathrm{final}} \\ \psi_{6_\mathrm{final}} \\ \psi_{7_\mathrm{final}} \end{bmatrix} = \hat{U} \begin{bmatrix} \psi_0 e^{-i\omega_0 t_d} \\ \psi_1 e^{-i\omega_1 t_d} \\ \psi_2 e^{-i\omega_2 t_d} \\ \psi_3 e^{-i\omega_3 t_d} \\ \psi_4 e^{-i\omega_4 t_d} \\ \psi_5 e^{-i\omega_5 t_d} \\ \psi_6 e^{-i\omega_6 t_d} \\ \psi_7 e^{-i\omega_7 t_d} \end{bmatrix} \tag{3.8}$$

We take the square of the wavefunction to obtain the state probabilities. 3.4 shows us the probabilities of being in each state after a two pulse sequence. We can excite to the desired state with 25% chance while keeping the undesired excitation to about 1% chance.

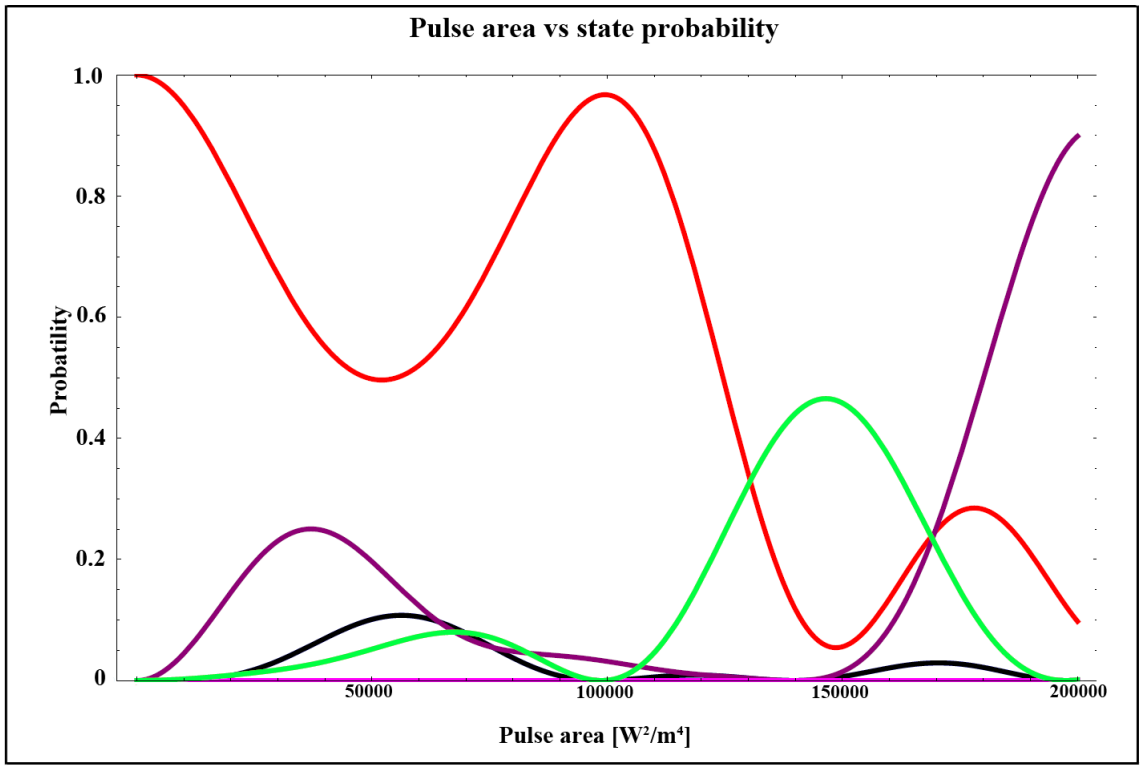

Figure 3.4: The purple curve represents ${}^2\mathrm{P}_{1/2}\,|F=0\rangle$, red curve is ${}^2\mathrm{S}_{1/2}\,|F=1,m_F=0\rangle$, green curve is ${}^2\mathrm{P}_{1/2}\,|F=1,m_F=+1\rangle$, magenta is ${}^2\mathrm{P}_{1/2}\,|F=1,m_F=0\rangle$, black is ${}^2\mathrm{S}_{1/2}\,|F=1,m_F=+1\rangle$. The undesired states are the green curve. We would like to maximize our probability of being in the purple curve while minimizing the probability of being in the green curve. The parameters chosen for calculation are $t_\mathrm{d}=237$ ps, $\tau=10$ ps. Initial starting state is red curve.

3.2 $^{174}\mathrm{Yb}^+$ Ramsey sequence

We have discussed how a sequence of pulses can shape the frequency spectrum that the ion sees. Before experimenting on $^{171}\mathrm{Yb}^+$ ions, we conducted a Ramsey experiment on $^{174}\mathrm{Yb}^+$ [24]. A Ramsey experiment is typically used to measure transition frequencies precisely. Consider a 2 level system starting in the ground state interacting with a series of pulses. First $\frac{\pi}{2}$ pulse excites the ground state to an even superposition of ground and excited state. Next, the atom is allowed to freely evolve for a time t_d. After free evolution, the atom is once again excited with a second $\frac{\pi}{2}$ pulse.

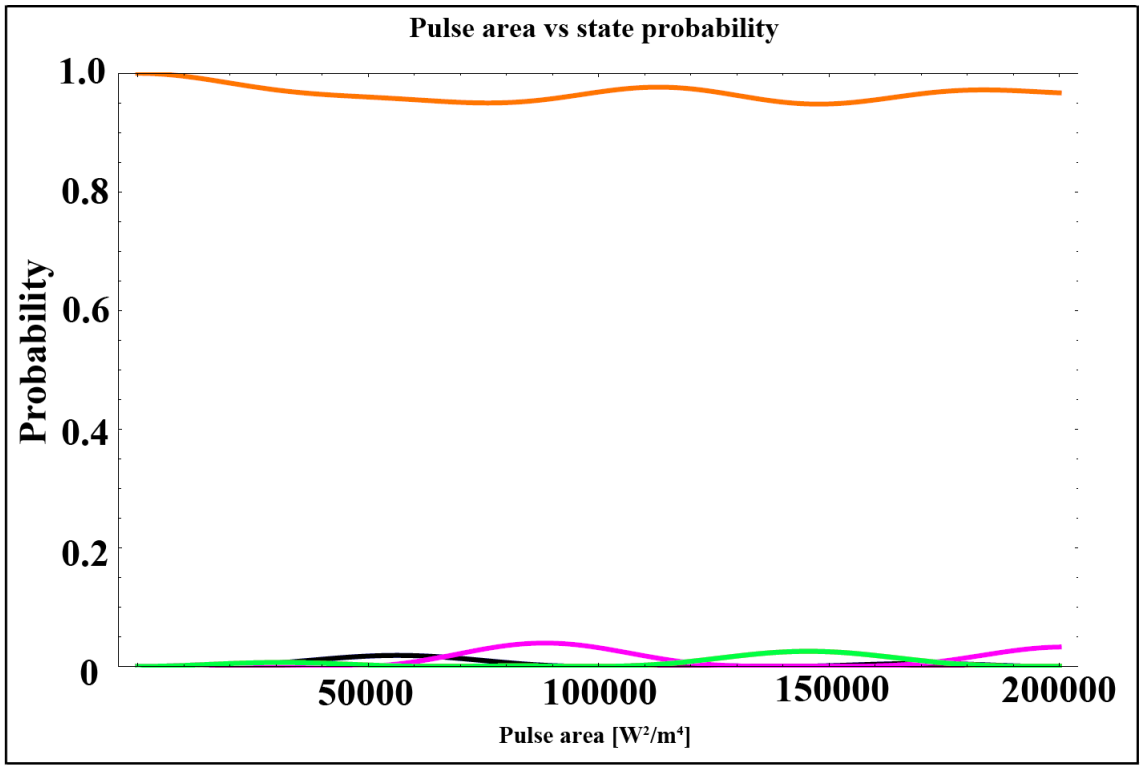

Figure 3.5: Plot of probability of being in each state vs pulse area with starting initial state being the dark state ${}^2\mathrm{S}_{1/2}\,|F=0,m_F=0\rangle$. Orange curve is ${}^2\mathrm{S}_{1/2}\,|F=0,m_F=0\rangle$,green curve is ${}^2\mathrm{P}_{1/2}\,|F=1,m_F=+1\rangle$, magenta is ${}^2\mathrm{P}_{1/2}\,|F=1,m_F=0\rangle$, black is ${}^2\mathrm{S}_{1/2}\,|F=1,m_F=+1\rangle$

Depending on the the timing of t_d, there will be interference resulting in what's called Ramsey fringes.

An optical delay stage creates the pulse pair by splitting the input pulse into two pulses with one arm of the delay stage being slightly longer than the other arm. The amount of delay is controlled by a piezoelectric motor mounted to a translation stage. Ytterbium ions have an excited state lifetime of 8 ns, and our repitition rate of our mode-locked laser is 12.5 ns. We would not only have to take into account the interaction of the ion with a pair of pulse that is seperated by 100s ps, but also the following pulse pair that arrives 12.5 ns later.

Let us calculate the effects of having a 4 pulse sequence, one pair that is

100s ps apart followed by a pulse pair that arrives 12.5 ns later. Once again, we utilize the density matrix to solve for the behavior of our 2 level system. Using equation 2.4 and assuming the ion starts in the ground state, the density matrix after the 1st pulse is

$$\rho^{(1)} = \begin{pmatrix} \cos(\frac{\theta}{2}) & i\sin(\frac{\theta}{2}) \\ i\sin(\frac{\theta}{2}) & \cos(\frac{\theta}{2}) \end{pmatrix} \begin{pmatrix} 0 & 0 \\ 0 & 1 \end{pmatrix} \begin{pmatrix} \cos(\frac{\theta}{2}) & -i\sin(\frac{\theta}{2}) \\ -i\sin(\frac{\theta}{2}) & \cos(\frac{\theta}{2}) \end{pmatrix} \tag{3.9}$$

$$= \begin{pmatrix} \sin^2(\frac{\theta}{2}) & \frac{i}{2}\sin(\theta) \\ -\frac{i}{2}\sin(\theta) & \cos^2(\frac{\theta}{2}) \end{pmatrix} \tag{3.10}$$

Followed by free evolution for a time t_{d}

$$\rho^{(1)}(t_{\mathrm{d}}) = \begin{pmatrix} \sin^2(\frac{\theta}{2})e^{-\gamma t_{\mathrm{d}}} & \frac{i}{2}\sin(\theta)e^{-\gamma/2t_{\mathrm{d}}}e^{-i\omega_{eg}t_{\mathrm{d}}} \\ -\frac{i}{2}\sin(\theta)e^{-\gamma/2t_{\mathrm{d}}}e^{-i\omega_{eg}t_{\mathrm{d}}} & \cos^2(\frac{\theta}{2})e^{-\gamma t_{\mathrm{d}}} \end{pmatrix} \tag{3.11}$$

Where ω_{eg} is the angular frequency between the ground and excited state. The next pulse arrives,

$$\rho^{(2)} = \begin{pmatrix} \cos(\frac{\theta}{2}) & i\sin(\frac{\theta}{2}) \\ i\sin(\frac{\theta}{2}) & \cos(\frac{\theta}{2}) \end{pmatrix} \rho^{(1)}(t_{\mathrm{d}}) \begin{pmatrix} \cos(\frac{\theta}{2}) & -i\sin(\frac{\theta}{2}) \\ -i\sin(\frac{\theta}{2}) & \cos(\frac{\theta}{2}) \end{pmatrix} \tag{3.12}$$

and $t_{\mathrm{rep}} = 12.5$ ns later,

$$\rho^{(2)}(t_{\mathrm{rep}}) = \begin{pmatrix} \rho^{(2)}_{ee}e^{-\gamma t_{\mathrm{rep}}} & \rho^{(2)}_{eg}e^{-\gamma/2t_{\mathrm{rep}}}e^{-i\omega_{eg}t_{\mathrm{rep}}} \\ \rho^{(2)}_{ge}e^{-\gamma/2t_{\mathrm{rep}}}e^{-i\omega_{eg}t_{\mathrm{rep}}} & (1-\rho^{(2)}_{ee}e^{-\gamma t_{\mathrm{rep}}}) \end{pmatrix} \tag{3.13}$$

where we have used the fact that $\rho_{ee} + \rho_{gg} = 1$. Pulse 3 arrives, giving us

$$\rho^{(3)} = \begin{pmatrix} \cos(\frac{\theta}{2}) & i\sin(\frac{\theta}{2})e^{-i\phi} \\ i\sin(\frac{\theta}{2})e^{i\phi} & \cos(\frac{\theta}{2}) \end{pmatrix} \begin{pmatrix} \rho_{ee}^{(2)} e^{-\gamma t_{\text{rep}}} & \rho_{eg}^{(2)} e^{-\gamma/2 t_{\text{rep}}} e^{-i\omega_{eg} t_{\text{rep}}} \\ \rho_{ge}^{(2)} e^{-\gamma/2 t_{\text{rep}}} e^{-i\omega_{eg} t_{\text{rep}}} & (1 - \rho_{ee}^{(2)} e^{-\gamma t_{\text{rep}}}) \end{pmatrix} \times \begin{pmatrix} \cos(\frac{\theta}{2}) & -i\sin(\frac{\theta}{2})e^{-i\phi} \\ -i\sin(\frac{\theta}{2})e^{i\phi} & \cos(\frac{\theta}{2}) \end{pmatrix} \tag{3.14}$$

We have allowed for the carrier envelope phase (CEP) to change between pulse to pulse coming out of the mode-locked laser. ϕ represents the CEP. Free evolution for a time of t_{d} gives us,

$$\rho^{(3)}(t_d) = \begin{pmatrix} \rho_{ee}^{(3)} e^{-\gamma t_{\text{d}}} & \rho_{eg}^{(3)} e^{-\gamma/2 t_{\text{d}}} e^{-i\omega_{eg} t_{\text{d}}} \\ \rho_{ge}^{(3)} e^{-\gamma/2 t_{\text{d}}} e^{-i\omega_{eg} t_{\text{d}}} & (1 - \rho_{ee}^{(3)} e^{-\gamma t_{\text{d}}}) \end{pmatrix} \tag{3.15}$$

The final pulse arrives resulting in

$$\rho^{(4)} = \begin{pmatrix} \cos(\frac{\theta}{2}) & i\sin(\frac{\theta}{2})e^{-i\phi} \\ i\sin(\frac{\theta}{2})e^{i\phi} & \cos(\frac{\theta}{2}) \end{pmatrix} \begin{pmatrix} \rho_{ee}^{(3)} e^{-\gamma t_{\text{d}}} & \rho_{eg}^{(3)} e^{-\gamma/2 t_{\text{d}}} e^{-i\omega_{eg} t_{\text{d}}} \\ \rho_{ge}^{(3)} e^{-\gamma/2 t_{\text{d}}} e^{-i\omega_{eg} t_{\text{d}}} & (1 - \rho_{ee}^{(3)} e^{-\gamma t_{\text{d}}}) \end{pmatrix} \times \begin{pmatrix} \cos(\frac{\theta}{2}) & -i\sin(\frac{\theta}{2})e^{-i\phi} \\ -i\sin(\frac{\theta}{2})e^{i\phi} & \cos(\frac{\theta}{2}) \end{pmatrix} \tag{3.16}$$

The numerical results show that instead of having a simple sinusoidal behavior expected from a Ramsey experiment, there's a more complex behavior that depends on the pulse area, CEP, and when the 2nd pair of pulse arrives relative to the excited state lifetime. As can be seen in figure 3.6, if the 2nd pair of pulse arrives at a time comparable to the excited state

lifetime, then the coherence is not totally lost, and we observe coherent effects come into play.

Analyzing the dependence on how the pulse area and CEP affects the shape of the Ramsey sequence, we allow the system to reach steady state. This occurs at around 36 total pulses. In figures 3.7 and 3.8, there are 80 total pulses (40 pulse pairs). In figure 3.7, we can see that at a pulse area of $\pi/2$, the CEP does not have any effect on the shape of the Ramsey sequence. In figure 3.8, we have allowed for the pulse area to change and the Ramsey sequence starts to deviate from a simple sinusoidal shape as the pulse area moves away from $\pi/2$.

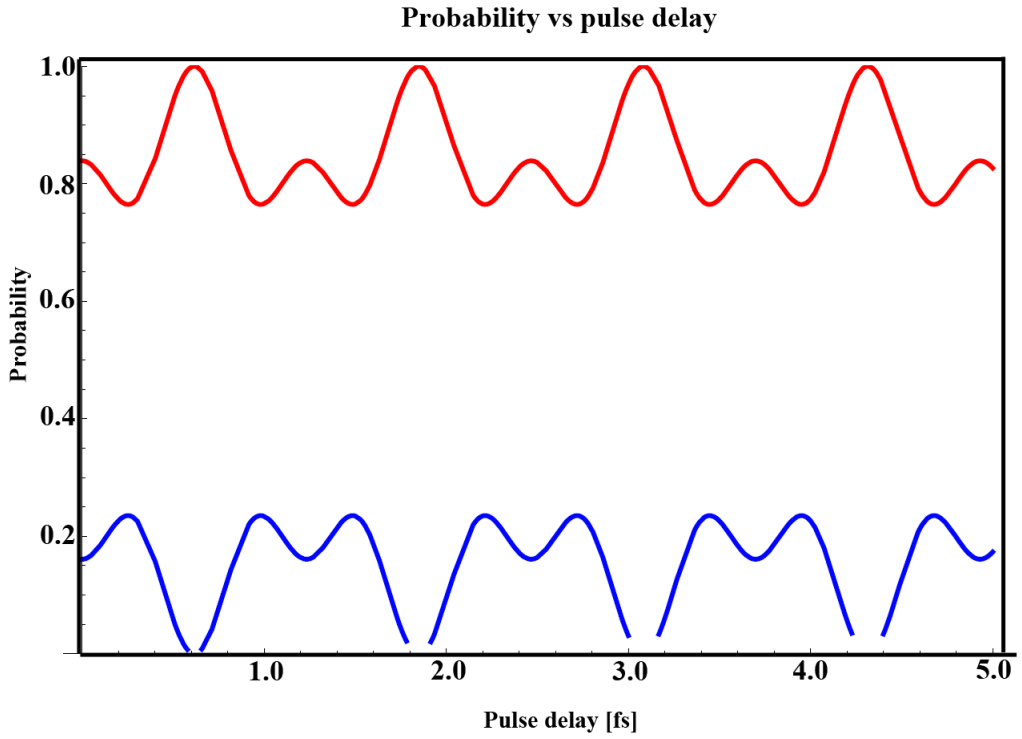

Figure 3.6: Blue curve corresponds to excited state, red curve corresponds to ground state. Parameters chosen are $\theta = \frac{\pi}{5}$, $t_{\text{rep}} = 12.5$ ns, $\omega_{eg} = 2\pi\times811.291400$ THz, $\gamma = 8$ ns, $\phi = 0$. Instead of a single period as expected from a Ramsey sequence, the comparable rate between the spontaneous decay and repetition rate of the mode-locked laser gives rise to a more complex behavior.

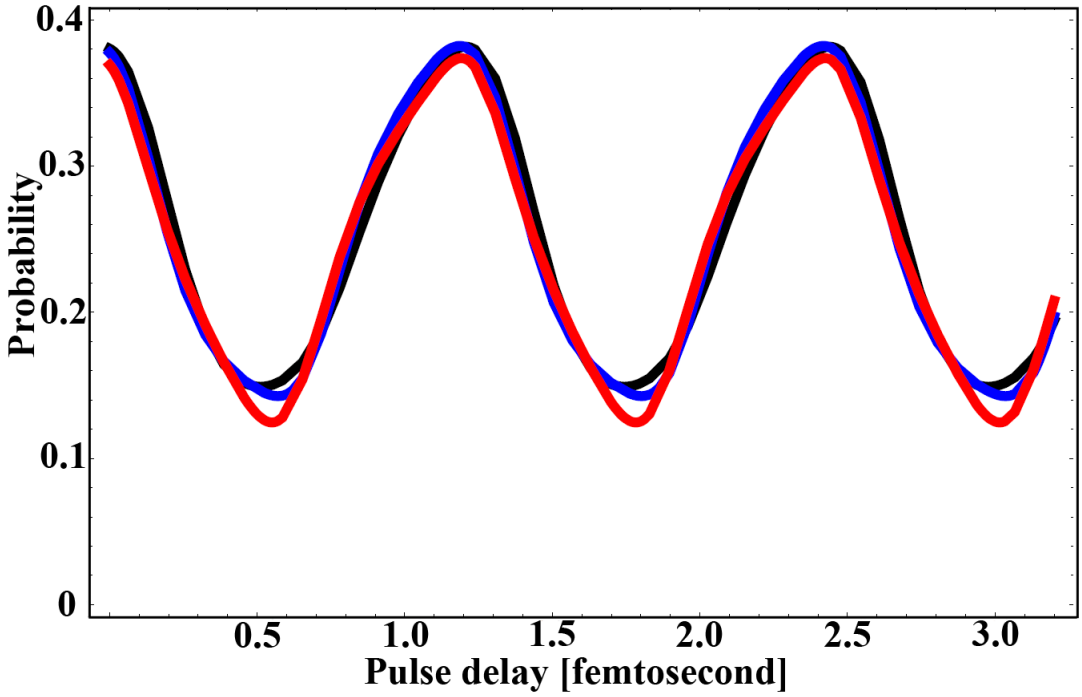

Figure 3.7: Plots of varying CEP for the excited state probability. Black Curve $\phi = \pi/2$, red curve $\phi = \pi/10$, blue curve $\phi = \pi/3$. Pulse area $\theta = \pi/2$ for all 3 curves.

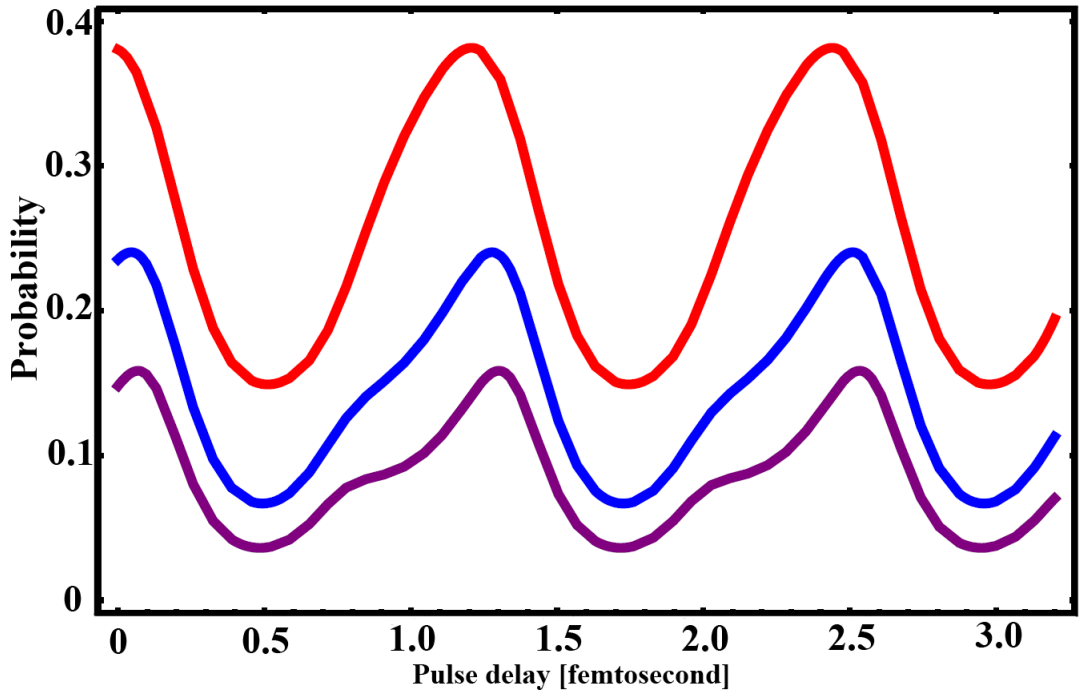

Figure 3.8: Plots of varying pulse area for the excited state probability. Red curve $\theta = \pi/2$, blue curve $\theta = \pi/3$, purple curve $\theta = \pi/4$.

CHAPTER 4

Results

Previously, two different groups have used pulsed lasers to Doppler cool trapped ions [14][13]. One experiment was done in the broadband regime where the excited state lifetime is much shorter compared to the time between pulses. The other experiment was operating in well resolved frequency comb regime where the repitition rate is 373 MHz compared to a 41 MHz transition linewidth. In our experiment, our repitition rate is ∼80 MHz, and our transition linewidth is ∼20 MHz.

We illuminate the ions with laser beams that are confined to the xy-plane. We collect fluorescence in the $-z$ direction with an imaging system that focuses onto a photon-counting photomultiplier tube (PMT) and intensified CCD camera. The ML laser is a standard, commercial, picosecond Ti:sapphire laser oscillator with a repetition rate of $f_{\mathrm{r}} = 1/T_{\mathrm{r}} = 81.553$ MHz. The center frequency of the laser is set to ~ 405.645 THz, and the output is frequency doubled via single-pass through a 0.8 cm LBO crystal cut for Type I phase matching for SHG of 760 nm light, generating an average UV power of around 9 mW at $\lambda \approx 369.5$ nm. The laser bandwidth ($> 10\,\mathrm{GHz}$) far exceeds the natural linewidth of ($1/\tau = 2\pi \times 19.7\,\mathrm{MHz}$) of the $^2P_{1/2}$ to $^2S_{1/2}$ transition in Yb^+.

For these parameters, the probability of the excited state decay between pulses ($1 - e^{-T_r/\tau}$) is 78%. Each decay will make the ion insensitive to the optical phase of the next pulse, suggesting that the comb teeth will not be resolved. The comb teeth visibility, $V \equiv \frac{(\Gamma_{\max} - \Gamma_{\min})}{(\Gamma_{\max} + \Gamma_{\min})}$ can help us quantify

how much coherent effects persists. From equation 2.43, we find

$$V = \cos^2\left(\frac{\theta}{2}\right)\mathrm{sech}\left(\frac{T_r}{2\tau}\right) \tag{4.1}$$

For our work, $V = 0.77$ which shows that despite the fact that the probability of decay is 78%, the inter-pulse coherent effects can still be seen fairly well.

The experimental procedure is as follows. We first load a $^{174}Yb^+$ ion with a 369 nm CW laser along with our 935 nm repumper. Then we micromotion compensate our ion by moving the ion to the RF null. This is done by iteratively moving the ion with our DC controls to minimize any micromotion bumps in the fluorescence linescan. We then turn off the 369 nm CW laser and turn on the ML laser to Doppler cool the ion. Each data point is taken at a rate of 100 ms per data point.

The results are shown in figure 4.1. As we scan the detuning of the mode-locked laser with a piezo inside the laser cavity, the fluorescence follows the rest-frame spectrum (red dashed curve) when the closest tooth is red detuned $\delta < 0$. Images of the ion are recorded periodically as the line scans are run. The left image in figure 4.1 shows a $^{174}Yb^+$ Doppler cooled near the ground state. The right image shows that the ion oscillates with a fixed amplitude as the nearest comb tooth becomes blue detuned $\delta > 0$. This fluorescence image matches well to the classical probability distribution of a harmonic oscillator convolved with the point-spread function of our imaging system. The fluorescence spectrum also departures drastically from the rest-frame spectrum. This is predicted by equation 2.47 as the secular-cycled average scattering rate depends on both the tooth detuning and amplitude of oscillation. To describe the fluorescence spectrum, we

calculate the average scattering rate over an oscillation period of the trap. This is done by numerically calculating equation 2.47 where if $\delta < 0$, $x_0 = 0$ and for $\delta > 0$, $x_0 = 4.9\,\mu$m.

The prediction of sustained large oscillation has been studied by a previous group where two CW laser light with one red detuned and one blue detuned of atomic resonance produced what's called a phonon laser [16]. We use this model, but instead substitute two colors of light, with a ML frequency comb. The derivation was done in previous section. The result is that the damping coefficient $\beta(E)$ changes sign with δ across resonance. If the closest comb tooth to resonance is red-detuned, $\beta > 0$, it can Doppler cool the ion's motion just like a CW laser. Equation 2.48 predicts a steady-state oscillation amplitude of $x_0 = 90$ nm for $\delta = -\pi/2T_r$, much smaller than the resolution ($\approx 1\mu$m) of the imaging system. We confirm theoretically that even with substantial spontaneous decay between pulses, the comb structure is sufficiently robust that the cooling effect of the nearest tooth is able to overcome the amplification induced by the rest of the spectrum. When the closest tooth is blue-detuned ($\delta > 0$), there will be net gain for the ion's motion from the laser field ($\beta < 0$). The frequency comb will add energy to the motion of an initially cold ion until the net power transfer is zero, resulting in steady-state oscillation as shown in 4.1. Multiple stable fixed points exists for 2.48 for both signs of δ. The fixed points are denoted by green dots in figure 2.2.

Figures 4.2 and 4.3 show the experimental signature of multiple fixed point solutions for the oscillation amplitude when the near-resonant tooth is red or blue detuned. These integrated fluorescence images resemble the "two-lobe" shape of an image of a classical harmonic oscillator probability distribution convolved with the point spread function of our imaging system. The fits are used to extract the oscillation amplitude fixed points

with a resolution-limited systematic uncertainty of ± 0.5 μm. When the near-resonant tooth is red detuned, We find stable oscillation amplitudes $(x_1^*, x_2^*, x_3^*) = (8.6, 16.9, 25.0)$ μm, compared to the theoretical prediction of $(9.7, 18.4, 27.5)$ μm from the roots of equation 2.48. For the blue-detuned case, we find $(x_1^*, x_2^*, x_3^*) = (4.9, 12.7, 20.7)$ μm, with the corresponding predicted values $(5.3, 14.0, 22.9)$ μm. The measured fixed points agree with the predicted values to about 10%.

We further verified that the system behaves as a phonon laser amplifier by acoustically injection locking [16] each of the first three fixed points (other than the $x_0^* \approx 0$ fixed point for $\delta < 0$) for both signs of δ. Using an aperature in the imaging system, ion fluorescence is collected from only one of the classical turning points in space, and the photons are time-tagged [15]. Figure 4.4 shows a numerical discrete Fourier transform of the recorded photon signal in the region near the secular frequency of the ion when it is in the lowest fixed point for blue detuning. A narrow peak (orange) appears at the frequency of a small sinusoidal voltage that was applied to one of the trap electrodes (injected signal), and the broad peak is the free-running phonon laser spectrum. When the injected oscillation frequency is within the phonon laser's gain profile, almost all of the gain is dedicated to amplifying the injected signal, and the phonon laser locks on to the injected signal in frequency and phase [42].

4.1 Ramsey sequence $^{174}Yb^{+}$

As discussed in the previous chapter, we have performed a series of Ramsey experiment on $^{174}Yb^{+}$ as a diagnostic before applying it to $^{171}Yb^{+}$. In figure 3.6 is the schematic of the experimental setup. 740 nm mode-locked light is shined onto a LBO crystal to generate 369 nm light. Each pulse is split into two pulses by a beam splitter with one leg passing through

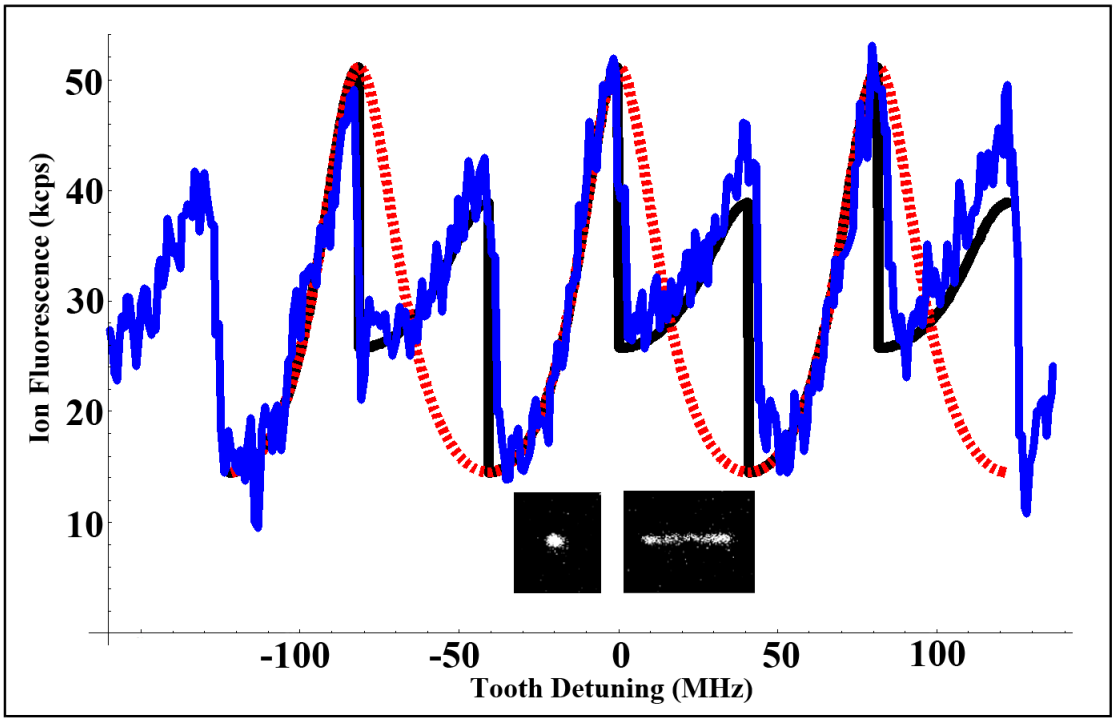

Figure 4.1: Blue curve is scanning ML laser detuning relative to atomic resonance. Red dashed curve is theoretical rest-frame lineshape. The solid black curve is equation 2.47 (red detuned corresponds to $x_0 = 0$, blue detuned corresponds to $x_0 = 4.9\,\mu$m). Depending on where the closest tooth lies, the spectrum will take on either the natural rest-frame resonance shape if the closest tooth is red, or it will departure from the rest-frame resonance shape if the closest tooth is blue detuned. The ion is seen to be Doppler cooled near the ground state (left image) when the closest tooth is red detuned. If the closest tooth is blue detuned, the ion can be seen oscilating with a fix amplitude (right image).

a delay stage with a piezo mounted to a mirror, while the other pulse is unaffected. The two pulses are recombined and sent to the ion. The result is that the ion sees a frequency spectrum that is carved out depending on the time delay between the two pulses. A RF spectrum is recorded by a fast photodiode of the pulse pair. Depending on where the time delay, the nodes will occur at different frequencies. As discussed in the previous chapter, the complication arises with multiple pulse pairs interacting with

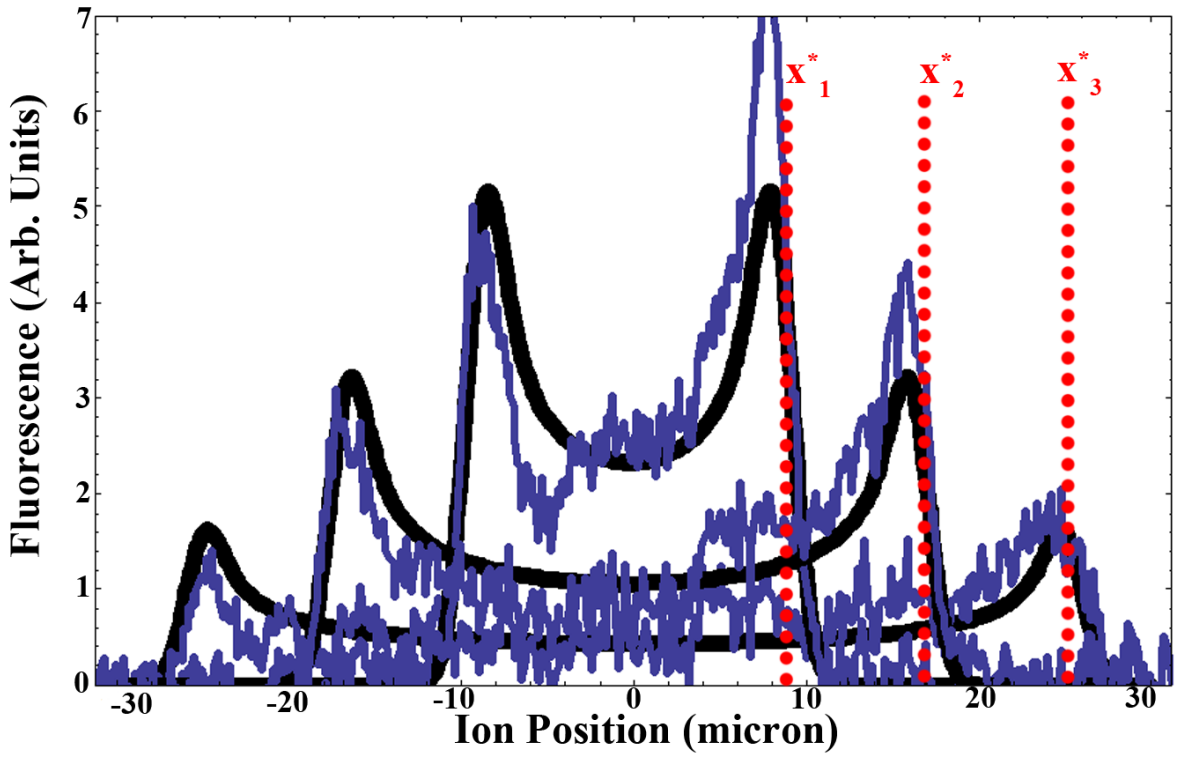

Figure 4.2: Integrated spatial images of fluorescence from an ion illuminated by an optical frequency comb whose nearest-resonant tooth is red detuned from rest-frame resonance. x_i^* represents the fixed points extracted from fitting a classical harmonic oscillator distribution convolved with the point spread function. $\delta/2\pi = -f_r/4$

the ion before the ion can fully relax due to the comparable time scales between the spontaneous decay rate and the mode-locked repitition rate. The result is shown in figure 4.6. The data fits to a sinusoidal function with a frequency corresponding to the energy splitting between the ${}^1S_0 \rightarrow {}^2P_0$ transtion. The sinusoidal behavior of the Ramsey experiment suggests that we have a pulse area of $\theta \approx \pi/2$. For a beam waist of $\omega_0 = 25$ μm, a $\pi/2$ pulse corresponds to about 400 μW of time averaged power.

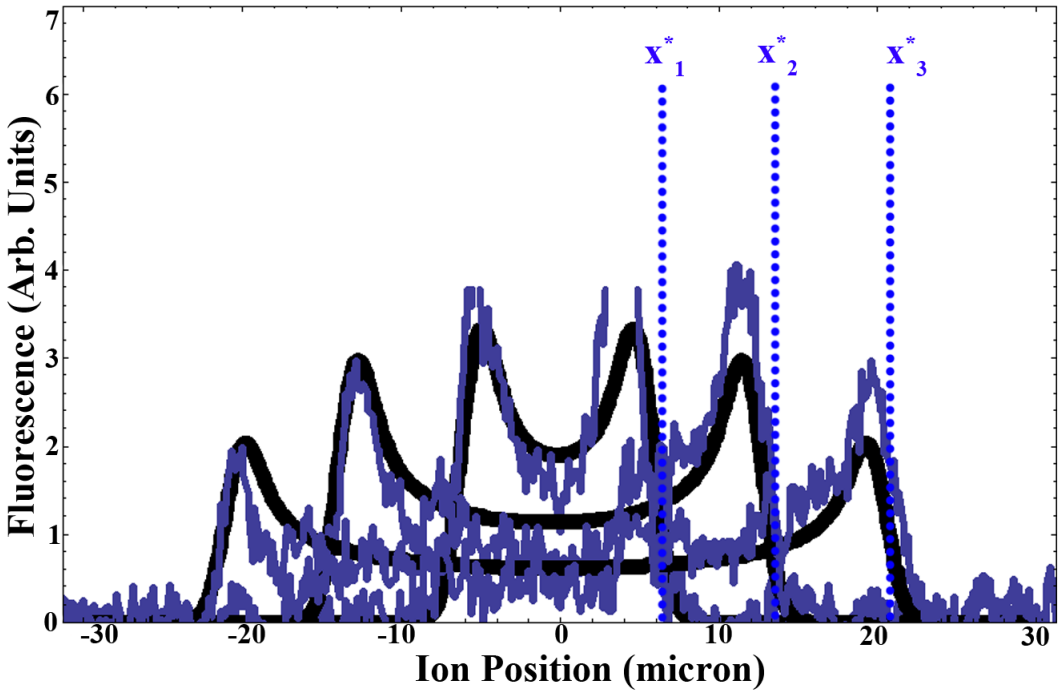

Figure 4.3: Integrated spatial images of fluorescence from an ion illuminated by an optical frequency comb whose nearest-resonant tooth is blue detuned from rest-frame resonance. x_i^* represents the fixed points extracted from fitting a classical harmonic oscillator distribution convolved with the point spread function. $\delta/2\pi = f_r/4$

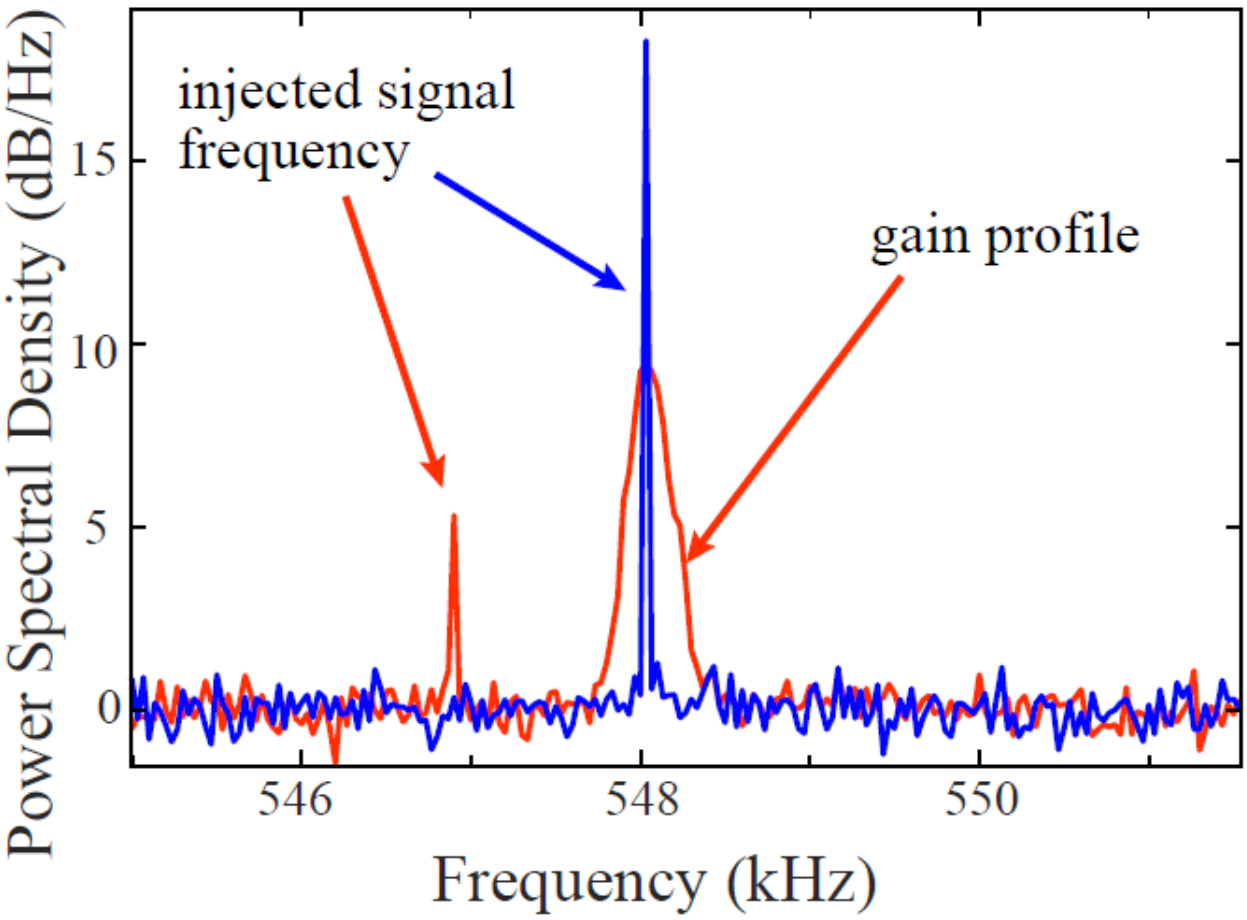

Figure 4.4: Acoustic injection locking of the x_1^* fixed point phonon laser when the near-resonant tooth is blue detuned. When the frequency of an injected signal is moved from outside (orange) to within (blue) the phonon laser's gain bandwidth, it is amplified at the expense of other frequencies.
.

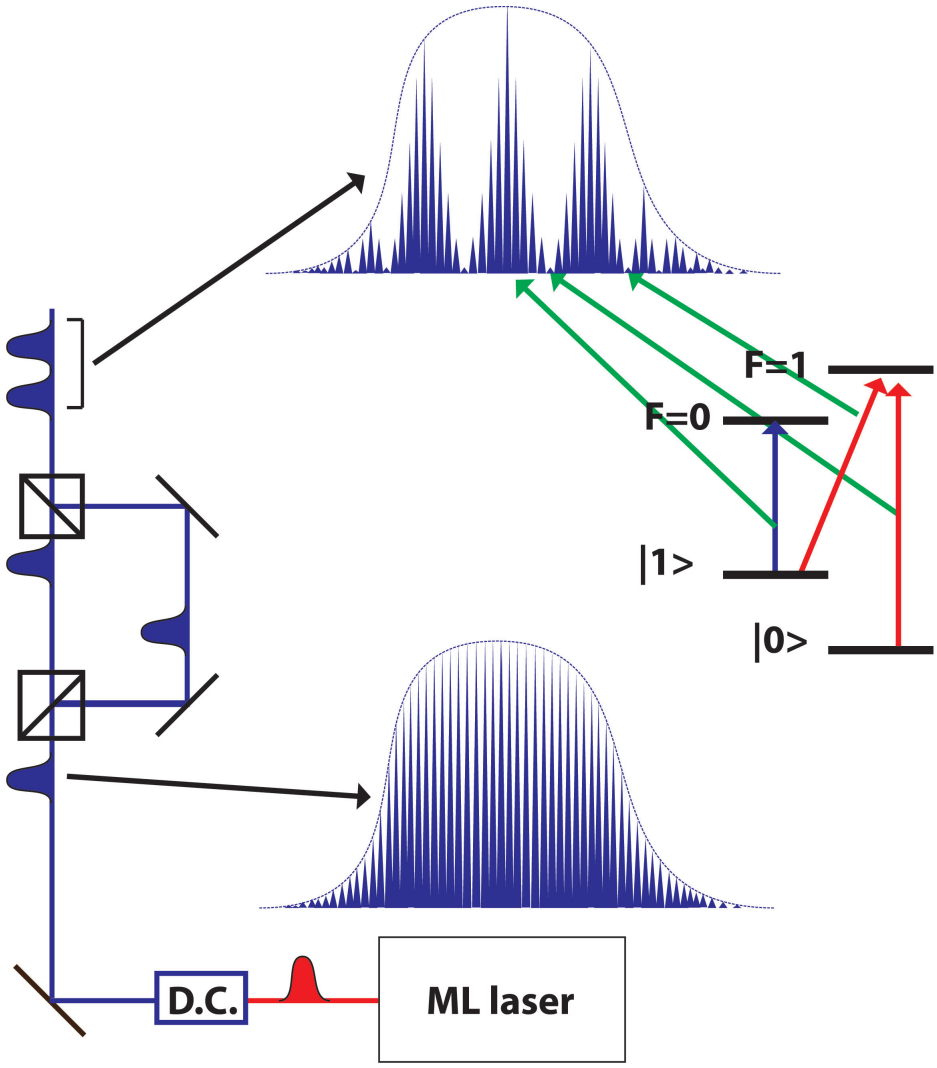

Figure 4.5: 740 nm light is frequency doubled to 369 nm by a LBO doubling crystal. The pulse gets split into two pulses by a beam splitter, with one pulse traveling on a slightly longer leg than the other by an optical delay stage. The recombined pulse is timed just right such that the red arrow transitions are sitting at a minima of the frequency comb, and the blue arrow transition sits at a peak.

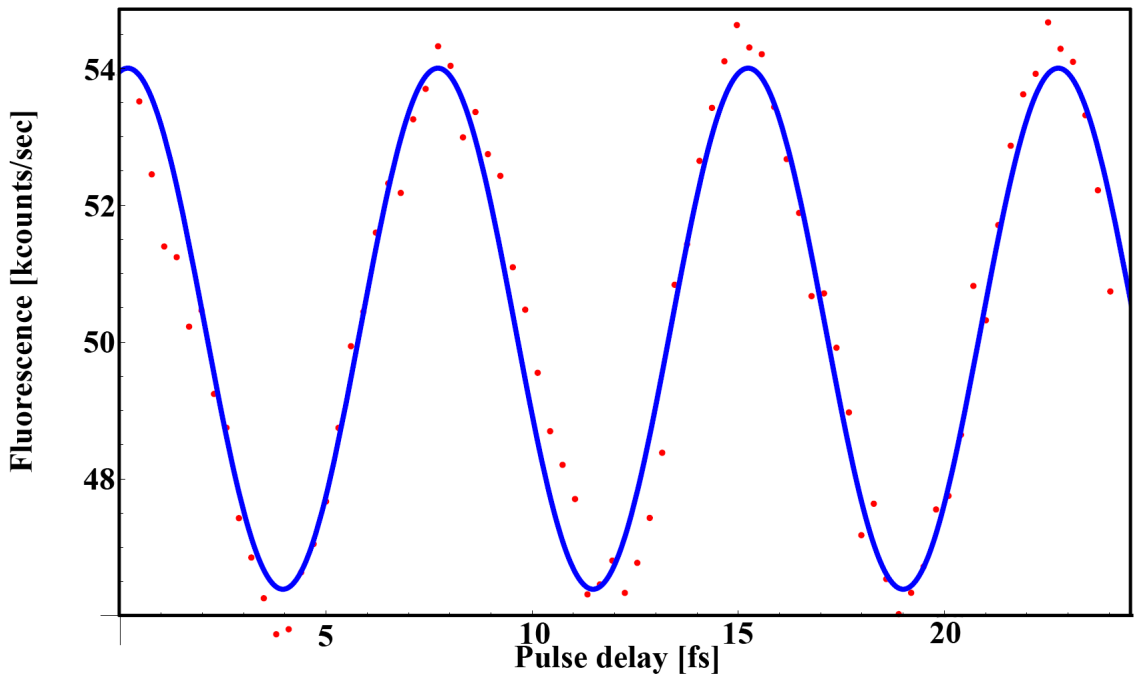

Figure 4.6: Ramsey experiment on $^{174}Yb^{+}$. Data is averaged over 5 different data sets.

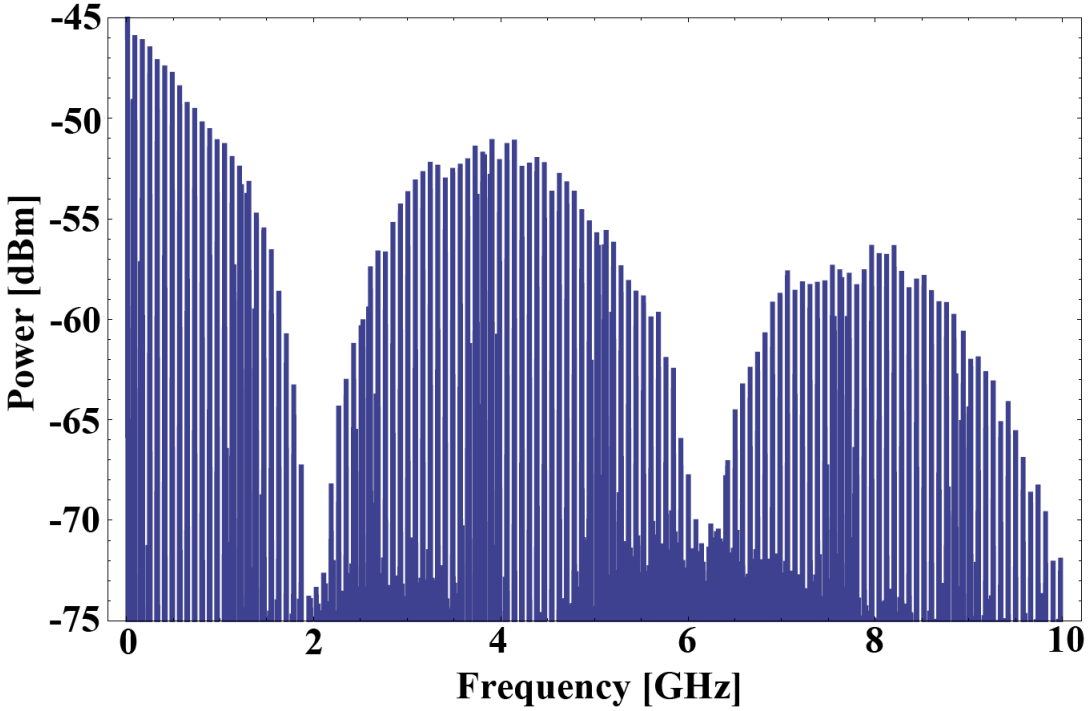

Figure 4.7: RF spectrum of pulse pair measured by a fast photodiode. By changing the amount of delay time between pulses, the node will occur at different frequencies. We choose a delay time of 237 ps so that there is a node at 2.1 GHz away. This is the optimal spot to perform the ultrafast state detection scheme for $^{171}Yb^{+}$.

.

CHAPTER 5

Conclusion and outlook

We have seen how a mode-locked laser can Doppler cool trapped ions. And also it can be used for state detection as well. The surprising fact that the blue-detuned teeth do not boil the ions out of the trap bodes well utilize a mode-locked laser to Doppler cool species that are even deeper in the UV regime. Species such as He^+ require 30 nm as the S to P cycling transition[37][38][39]. There is no CW light that can be produced in that wavelength as of now. Using a two-photon transition scheme, one can use light at 60 nm to Doppler cool He^+ [40]. This would mean we would need to frequency quadrupule light at 240 nm. Frequency quadrupuling wins if one were to use a CW laser, since the doubling efficiency scales as the instantaneous intensity.

As for the ultrafast state detection scheme, it is also not obvious initially that having color everywhere would be possible to state detect, since it is important to not off resonantly scatter into an undersired state. But if the frequency spectrum is carved out properly with an optical delay stage, it can potentially prove to be a useful and novel way for state detection.

REFERENCES

[1] R. Blatt and D. Wineland, Nature, 453:1008 (2008) *"Entangled states of trapped atomic ions"*

[2] D.J. Wineland, C. Monroe, W.M. Itano, D. Leibfried, B.E. King, D.M. Meekhof, Journal of Research of the National Institute of Standards and Technology, 103, 259 (1998) *"Experimental Issues in Coherent Quantum-State Manipulation of Trapped Atomic Ions"*

[3] W.M. Itano and D. Wineland, PRA 25, 1 (1982) *"Laser cooling of ions stored in harmonic and Penning traps"*

[4] D. Das et al., PRA 72, 032506 (2005) *"Absolute frequency measurements in Yb with 0.08 ppb uncertainty: Isotope shifts and hyperfine structure in the 399 nm* $^1S_0 \rightarrow^1 P_1$ *line"*

[5] A. S. Bell et al., PRA 44, 1 (1991) *"Laser cooling of trapped ytterbium ions using four-level optical-excitation scheme"*

[6] E. Ilinova et. al., PRA 84, 033421 (2011) *"Doppler cooling with coherent trains of laser pulses and a tunable velocity comb"*

[7] D. Felinto et al., Optics Communications 215, 69-73 (2003) *"Coherent accumulation in two-level atoms excited by a train of ultrashort pulses"*

[8] D. Aumiler et. al., PRA 85, 063412 (2012) *"Simultaneous laser cooling of multiple atomic species using an optical frequency comb"*

[9] K. Vahala et al., Nature Physics Vol. 5, 10.1038, (2009 *"A phonon laser"*

[10] A.E. Siegman. Lasers. University Science Books, Sausalito, CA, 1986.

[11] D. Leibfried, R. Blatt, C. Monroe, D. Wineland, Reviews of Modern Physics, Vol. 75, (2003) *Quantum dynamics of single trapped ions*

[12] Pradip Ghosh, *Ion Traps*, Oxford Science Publications, 1995

[13] B.B. Blinov, R.N. Kohn Jr., M.J. Madsen, P. Maunz, D.L. Moehring and C. Monroe, J. Opt. Soc. Am. B 23, 1170 (2006)

[14] J. Davilla-Rodriguez, A. Ozawa, T. W. Hansch, and T. Udem, PRL. 116, 043002 (2016)

[15] T. Pruttivarasin and H. Katori, Rev. Sci. Instrum. 86, 115106 (2015)

[16] S. Knunz, M. Herrmann, V. Batteiger, G. Saathoff, T.W. Hansch, K. Vahala, and Th. Udem, Physical Review Letters, Vol 105, 013004 (2010)

[17] Paul, Wolfgang, Reviews of Modern Physics. 62 (3): 531540. (1990) *Electromagnetic Traps for Charged and Neutral Particles*

[18] R. P. Feynman,International Journal of Theoretical Physics 21, 467 (1982). *Simulating physics with computers*

[19] R. Blatt and D. J. Wineland, Nature 453, 1008 (2008). *Entangled states of trapped atomic ions*

[20] W. B. Cairncross, D. N. Gresh, M. Grau, K. C. Cossel, T. S. Roussy, Y. Ni, Y. Zhou, J. Ye, E. A. Cornell, Phys. Rev. Lett. 119, 153001 (2017) *A precision measurement of the electron's electric dipole moment using trapped molecular ions*

[21] John J. Bollinger, D J. Heinzen, F L. Moore, Wayne M. Itano, David J. Wineland, Physica Scripta. (OCTOBER 01, 1992) *Low Order Modes of an Ion Cloud in a Penning Trap*

[22] Morse. Philip McCord, Feshbach. Herman, Boston, Mass: McGraw-Hill Inc.,US. ISBN 9780070433168.(1953-01-01). *Methods of Theoretical Physics: Pt. 1*

[23] Bryce Yoshimura, Marybeth Stork, Danilo Dadic, W. C. Campbell, J. K. Freericks. EPJ Quantum Technology 2, 2 (2015) *Creation of two-dimensional coulomb crystals of ions in oblate Paul traps for quantum simulations*

[24] Foot, C. J. (2005). Atomic Physics. Oxford University Press. ISBN 978-0-19-850696-6.

[25] Metcalf, H. J.; van der Straten, P. (1999). Laser Cooling and Trapping.

[26] W. W. Macalpine and R. O. Schildknecht, *Coaxial Resonators with Helical Inner Conductor*, Proc. IRE , 2099 (1959).

[27] D. J. Berkeland, J. D. Miller, J. C. Bergquist, W. M. Itano, and D. J. Wineland, Journal of Applied Physics 83, 5025 (1998) *Minimization of ion micromotion in a Paul trap*

[28] J. Mizrahi, B. Neyenhuis, K. G. Johnson, W. C. Campbell, C. Senko, D. Hayes, C. Monroe, Applied Physics B 114, 45 (2014). *Quantum Control of Qubits and Atomic Motion Using Ultrafast Laser Pulses*

[29] C. Monroe, D. Meekhof, B. King, W. Itano, and D. Wineland, Phys. Rev. Lett. 75, 4714 (1995). *Demonstration of a Fundamental Quantum Logic Gate*

[30] G. Brassard, I. Chuang, S. Lloyd, and C. Monroe, Proc. Nat. Acad. Science 95,11032 (1998). *Quantum Computing*

[31] H. Hffner. Nature 465, 555, (2010). *Frustrated trio mimicked*

[32] David Hucul, Justin E. Christensen, Eric R. Hudson, and Wesley C. Campbell. Phys. Rev. Lett. 119, 100501 (2017) *Spectroscopy of a Synthetic Trapped Ion Qubit*

[33] T. Rosenband, D. B. Hume, P. O. Schmidt, C. W. Chou, A. Brusch, L. Lorini, W. H. Oskay, R. E. Drullinger, T. M. Fortier, J. E. Stalnaker, S. A. Diddams, W. C. Swann, N. R. Newbury, W. M. Itano, D. J. Wineland, and J. C. Bergquist, Science 319, 1808 (2008) *Frequency ratio of Al+ and Hg+ single-ion optical clocks; metrology at the 17th decimal place*

[34] T. Rosenband et al., Phys. Rev. Lett. 98, 220801 (2007) *Observation of the* $^1S_0$ *to* $^3P_0$ *transtion in* $^27Al^+$

[35] W. Neuhauser, M. Hohenstatt, P. Toschek, and H. Dehmelt, Phys. Rev. Lett. 41, 233 (1978). *Optical-Sideband Cooling of Visible Atom Cloud Confined in Parabolic Well*

[36] K. Kato, IEEE J. Quant. Elecr. QE-22, 1013 (1986). *Second-harmonic generation to 2048 Ba2O4*

[37] M. Herrman, M. Haas, U. D. Jentschura, F. Kottmann, D. Leibfried, G. Saatho, C. Gohle, A. Ozawa, V. Batteiger, S. Knunz, N. Kolachevsky, H. A. Schussler, T. W. Hansch, K. Vahala, and T. Udem, Phys. Rev. A 79, 052505 (2009). *Feasibility of coherent xuv spectroscopy on the 1S to 2S transition in singly ionized helium*

[38] A. Cingoz, D. C. Yost, T. K. Allison, A. Ruehl, M. E. Fermann, I. Hartl, and J. Ye, Nature 482, 68 (2012). *Direct frequency comb spectroscopy in the extreme ultraviolet*

[39] A. McPherson, G. Gibson, H. Jara, U. Johann, T. S. Luk, I. A. McIntyre, K. Boyer, and C. K. Rhodes, J. Opt. Soc. Am B. 4, 595 (1987) *Studies of multiphoton production of vacuum-ultraviolet radiation in the rare gases*

[40] D. Kielpinski, Phys. Rev. A 73, 063407 (2006). *Laser cooling of atoms and molecules with ultrafast pulses*

[41] A. M. Jayich, X. Long, and W. C. Campbell, Phys. Rev. X 6, 041004 (2016). *Direct Frequency Comb Laser Cooling and Trapping*

[42] A. Yariv and W. M. Caton, IEEE Journal of Quantum Electronics QE-10, 509 (1974) *Frequency, intensity, and field fluctuations in laser oscillators*